minerals

MDPI

Review

Updating Geological Information about the Metallogenesis of the Iberian Pyrite Belt

Reinaldo Sáez [1,*], Felipe González [1], Teodosio Donaire [1], Manuel Toscano [1], Lola Yesares [2], Gabriel Ruiz de Almodóvar [1] and Carmen Moreno [1]

[1] Earth Science Department, Avenida de Las Fuerzas Armadas, University of Huelva, 21071 Huelva, Spain; fbarrio@uhu.es (F.G.); donaire@uhu.es (T.D.); mtoscano@uhu.es (M.T.); almodovar@uhu.es (G.R.d.A.)
[2] Department of Mineralogy and Petrology, Universidad Complutense, 28040 Madrid, Spain; myesares@ucm.es
* Correspondence: saez@uhu.es

Abstract: The Iberian Pyrite Belt (IPB) represents one of the largest districts of volcanogenic massive sulfide (VMS) deposits in the world, and is a critical source of base metals (Cu, Pb, and Zn) for Europe. Confirmed resources exceed 1700 Mt of massive sulfides with grades of around 1.2% Cu, 1% Pb, and 3% Zn as well as more than 300 Mt of stockwork-type copper mineralization. Significant resources of Sn, precious metals (Au and Ag), and critical metals (Co, Bi, Sb, In, and Se) have also been evaluated. The genesis of these deposits is related to a complex geological evolution during the late Devonian and Mississippian periods. The geological record of such evolution is represented by three main lithological units: Phyllite–Quartzite Group, the volcano–sedimentary Complex (VSC), and the so-called Culm Group. The sulfide deposits are located in the VSC, associated with felsic volcanic rocks or sedimentary rocks such as black shales. The massive sulfide deposits occur as tabular bodies and replacement masses associated with both volcanic and sedimentary rocks. Their mineralogical composition is relatively simple, dominated by pyrite, chalcopyrite, sphalerite, and galena. Their origin is related to three evolutionary stages at increasing temperatures, and a subsequent stage associated with the Variscan deformation. The present paper summarizes the latest developments in the IPB and revises research areas requiring further investigation.

Keywords: Iberian Pyrite Belt; IPB; massive sulfide deposits; volcanogenic massive sulfides; VMS; black shales; volcanic rocks; metallogenesis; evolution; deformation

Citation: Sáez, R.; González, F.; Donaire, T.; Toscano, M.; Yesares, L.; de Almodóvar, G.R.; Moreno, C. Updating Geological Information about the Metallogenesis of the Iberian Pyrite Belt. *Minerals* **2024**, *14*, 860. https://doi.org/10.3390/min14090860

Academic Editors: Luís Albardeiro, Maria João Batista and Alejandro Díez-Montes

Received: 15 June 2024
Revised: 12 August 2024
Accepted: 18 August 2024
Published: 24 August 2024

1. Introduction

The Iberian Pyrite Belt (IPB) contains the world's largest concentration of massive sulfide deposits associated with volcanic rocks. Spanning approximately 8000 km^2 from southern Lisbon to the vicinity of Seville, the region also includes some of the largest known accumulations of volcanogenic massive sulfide (VMS) deposits in the Earth's crust (Figure 1) [1].

Original mineral resources have been estimated at around 2000 Mt, with 1700 Mt corresponding to massive sulfides and the remainder to stockwork-type mineralizations [1]. Evidence of mining exploitation in the region dates back over 5000 years, with several periods of intense mining activity. Throughout history, 82 sulfide deposits have been exploited to varying degrees, and numerous indications of deposits never mined have been documented [1–6].

Currently, favorable metal prices and advancements in mining and mineral processing techniques keep the mining province among the leading base metals producers in Europe. Currently, there are seven operational mining centers: five in Spain (Las Cruces, Riotinto, Sotiel, Magdalena, and Aguas Teñidas) and two in Portugal (Aljustrel and Neves-Corvo). Additionally, numerous projects are in the advanced exploration stages, including the following: Escacena (Panglobal Resources), Lomero-Poyatos (Denarius Metals), San Telmo

and Tharsis (Tharsis Mining) and La Infanta, El Cura, and Romanera (Emerita Resources). Some other projects are in the design and permitting phases for exploitation: Los Frailes (Grupo Mexico), Concepción (MATSA), and Masa Valverde (Atalaya Mining).

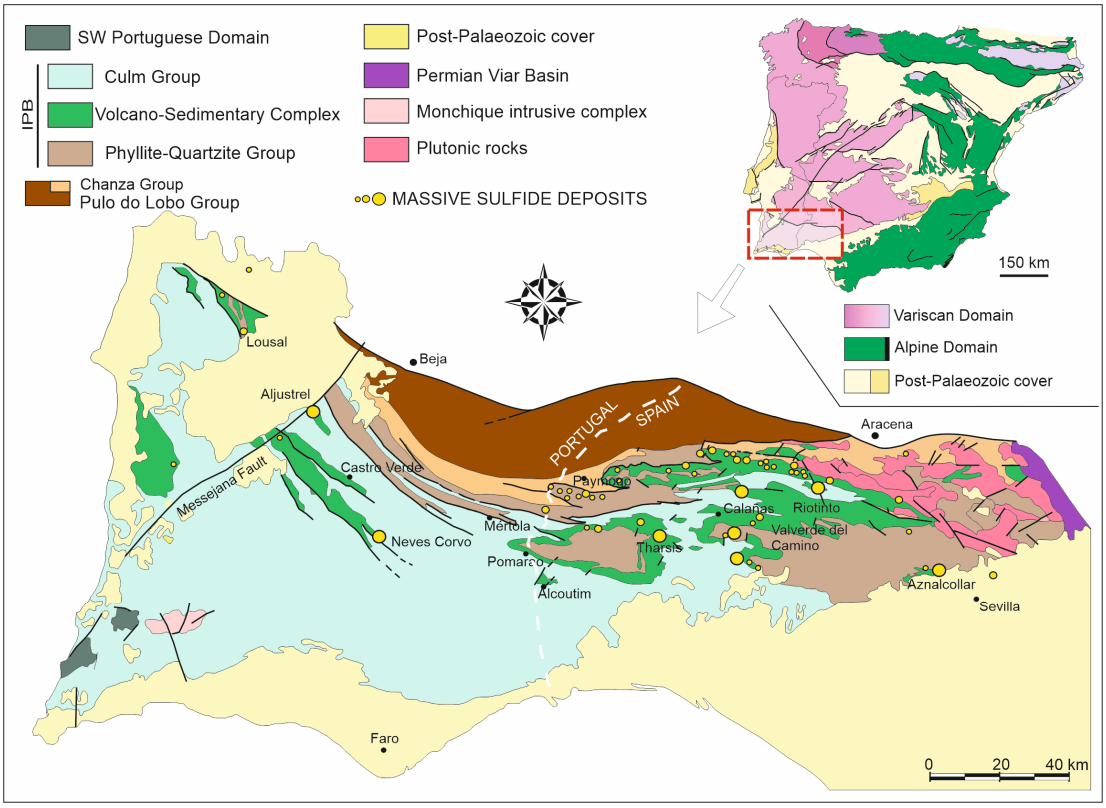

Figure 1. Geological sketch map of the IPB showing the location of the known VMS.

The abundance and diversity of massive sulfide deposits have garnered significant interest within the scientific community. Despite the extensive body of work published on various aspects of this metallogenic province, there is no general consensus unifying the knowledge of a region with such exceptional metallogeny. Initial genetic models debated two alternative models dominated by sedimentary processes or high-temperature hydrothermal fluid replacement (see Bateman [7] and the included references).

Since the mid-20th century, globally applicable metallogenic models for VMS deposits, both ancient and modern [8–10], have been widely applied for those in the IPB—see [11–15] and the included references. However, many questions still remain under debate. These include the geodynamic framework, depositional environment, metallogenetic processes, nature of hydrothermal fluids, sources of sulfur and metals, and the thermal engine driving regional-scale hydrothermalism. In order to compose a document covering the current state of knowledge on IPB metallogenesis that can be also useful as a conceptual basis and guide for future prospecting and exploration activities in the region, the present study reviews the main contributions to the geology and metallogeny of the IPB and proposes a synthesis model that integrates the aforementioned aspects.

2. Stratigraghy

The current concepts regarding the stratigraphy of the FPI are attributed to [16], who unified previous nomenclatures based on local descriptions, cartographies, or synthesis works [17–23] and grouped the outcropping rocks into three lithostratigraphic units of different ranks, denominated from bottom to top as follows: "Phyllite–Quartzite Group" (PQ), "Volcanic–Siliceous Complex (VS)" and "Culm Group". Currently, Schermerhorn's original terminology appears slightly modified in the literature: the Phyllite–Quartzite Group (PQ) is commonly referred to as the Shale and Quartzite Group, retaining the

acronym PQ; the Volcano–Siliceous Complex (VS) is cited as the volcanic and sedimentary complex (VSC), and the Culm Group maintains its nomenclature and meaning, although Portuguese authors often refer to it as the Baixo Alentejo Flysch Group. Figure 2 shows a schematic representation of the IPB lithostratigraphic series and Figure 3 illustrates the most representative sedimentary rocks in it.

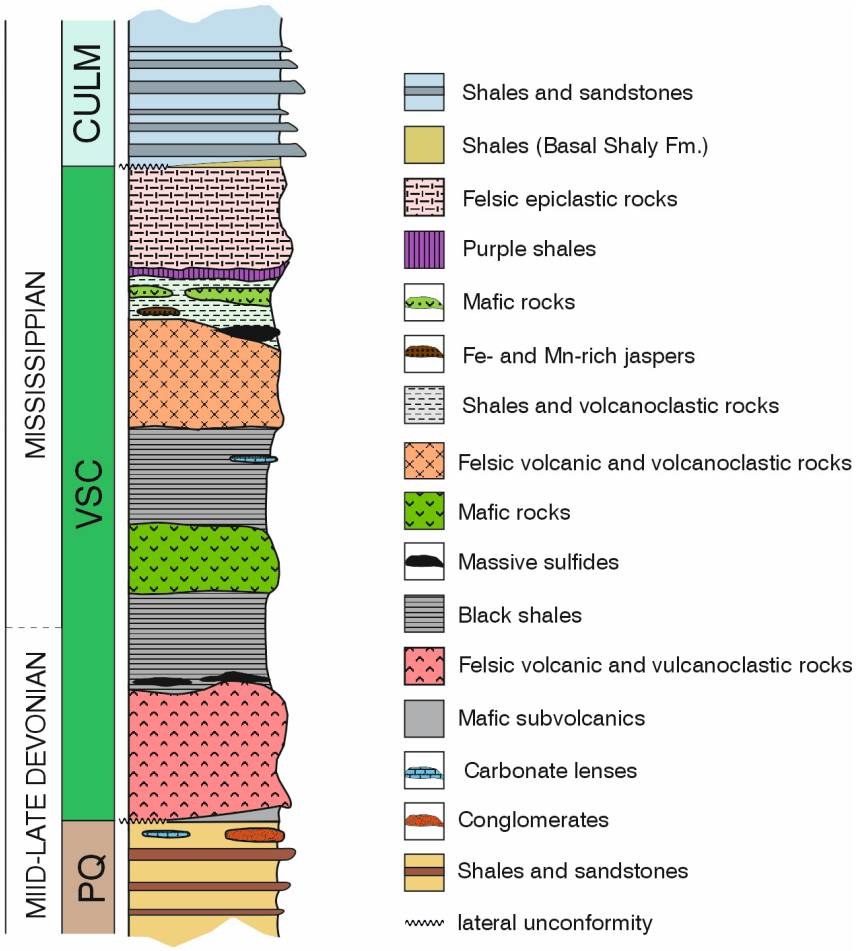

Figure 2. Generalized stratigraphic column of the IPB. Based on [24] and the references therein.

The PQ Group represents the base of the regional stratigraphic series. Its age has traditionally been assigned to the Late Devonian (late Famennian) period based on conodonts recovered from the carbonate levels occurring toward the top of the unit [23,25–27]. More recent palynological studies extend the chronological range of the PQ Group, increasing down the age of the rocks to the Givetian and specifying the age of its top as Strunian. Thus, with current data, the age of the outcropping rocks of the PQ Group ranges between the early Givetian and the topmost Famennian [28,29]. The Givetian age only applies to the oldest rocks dated so far. The age of the PQ Group base cannot be determined as the underlying formation does not outcrop. Such indeterminacy is also applied to the thickness, which has been tentatively estimated as more than 2000 m [21]. Its lithostratigraphic characteristics are consistent throughout the IPB and are very similar to those of its stratigraphic equivalent unit in the southwest Portuguese region (Tercenas Formation). Most of the stratigraphic series of the PQ Group, as well as the Tercenas Formation, is composed of dark shales (gray to black) with centimeter-thick layers of fine sandstones (quartz arenites and quartz wackes). Their facies represent deposition in a shallow marine environment [20], specifically in a shallow marine platform of low energy, sporadically affected by storms [30].

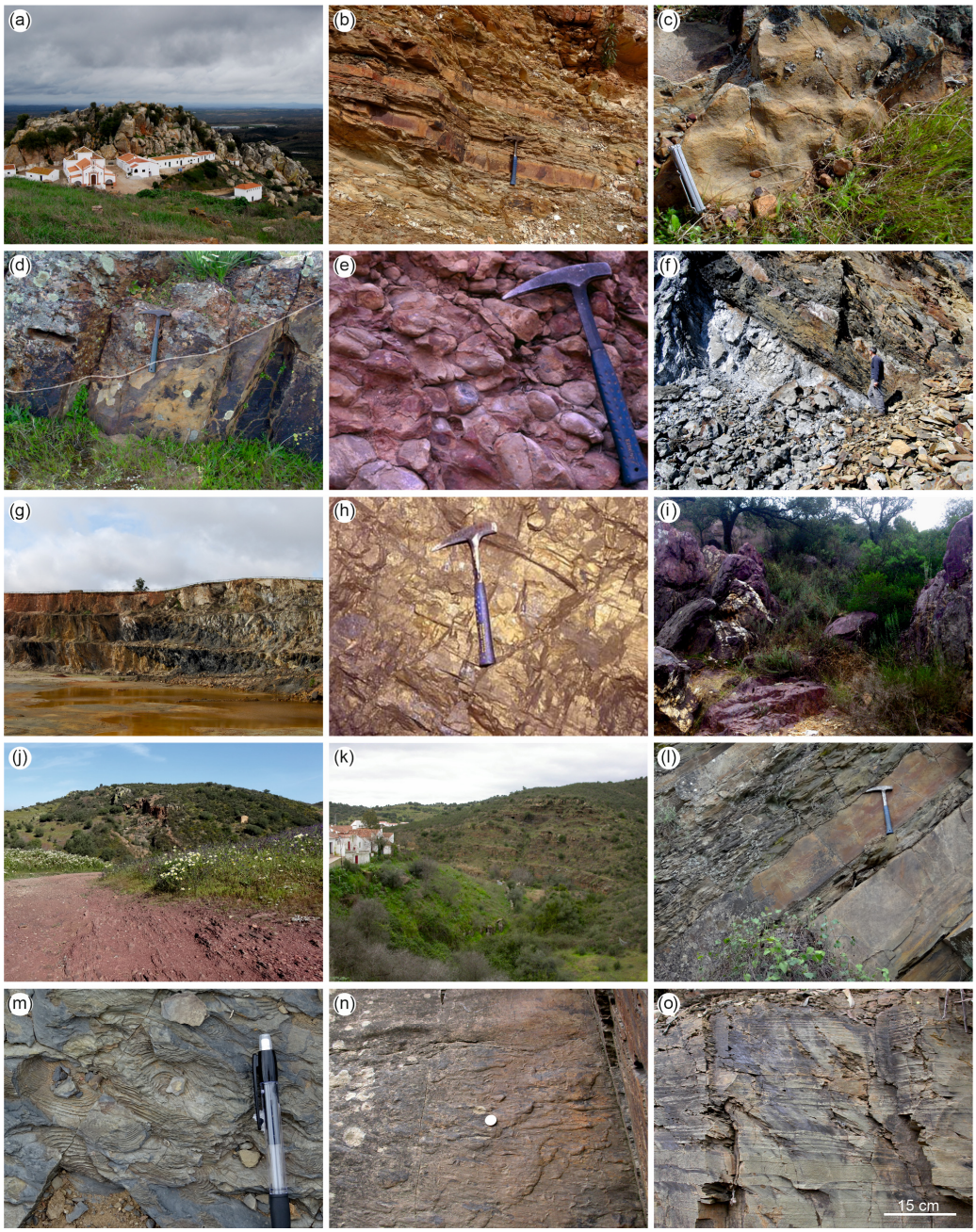

Figure 3. Sedimentary rocks at the IPB. (**a**,**e**) PQ Group; (**f**,**j**) volcano–sedimentary complex; (**k**) to (**o**) Culm Group. (**a**) Thick quartz–arenite levels from the top of the PQ Group standing out in the landscape, (**b**) shale–quartz–arenite succession; (**c**) linguoid ripples in quart–arenite layers; (**d**) conglomeratic channel intersecting sandstone bars; (**e**) conglomerates associated with gravity flow deposits; (**f**,**g**) black shales; (**h**) massive sulfide deposits; (**i**) Mn-rich jaspers; (**j**) purple shales in the foreground and Mn-rich jaspers in the background; (**k**) outcrop and (**l**) detail of the grauwacke–shale succession characteristic of the Culm Group; (**m**) accumulation of *Posidonia becherii* in a shale layer; (**n**) prod, bounce, and flute cast produced by turbiditic currents; (**o**) flaser, wavy, and lenticular bedding produced by disparate density currents.

A chronostratigraphic, though not strictly lithostratigraphic, correlation has also been established between the PQ Group and the youngest Devonian units of Pulo do Lobo (Santa Iria, Horta da Torre, and Represa Formations) [15]. During the Upper Devonian, the IPB, SW Portugal, and Pulo do Lobo must have belonged to the same realm. The latest Devonian crisis, representing the onset of the Variscan orogeny in the region, affected these three

areas in different ways, leading to the differentiation of such realms. The SW Portuguese Domain, distant from tectonic disturbances, remained as a siliciclastic and occasionally carbonate platform until the Bashkirian [31]. The IPB underwent a fragmentation process caused by transtensive tectonics, resulting in the creation of numerous basins with uneven sedimentation rates, the emergence of bimodal volcanism, and the formation of large volumes of massive sulfides (see below). The Pulo do Lobo, close to the convergence zone between the IPB and southern Iberia, was subjected to intense compressive activity from that time onward; see [32] and the references therein.

Toward the top of the PQ Group, there is an increase in the sand/lutite ratio, the thickness of sandstone beds, and the grain size of sandstones, resulting in a coarsening-upward sequence. The sandstones become the dominant lithofacies, representing the deposition of shoreline bars accumulated by wave action in a littoral environment that only occasionally shows the effect of tides [30,33]. Generally, there is a gradual basin shallowing, which locally favors subaerial exposure. This relative sea-level fall is a phenomenon described globally for the Late Devonian—see [34] and the references therein—that in the IPB coincides with the initial manifestations of the Variscan orogeny in the region. Thus, the top of the PQ Group is characterized by a mosaic of lithofacies, some of them indicative of highly energetic processes: slump deposits, mega-debris flows, deltaic fans, poorly developed reef patches, and the previously described shoreline bars [33]. The most representative outcrops are exposed in the area of Virgen de la Peña (Puebla de Guzmán, Huelva) and at Cabezo de Migollas, near the Sotiel Coronada mine (Calañas, Huelva) but outcrops showing these facies are scattered throughout the IPB [33,35].

At a global scale, the so-called "Late Devonian Crisis" [36] has been attributed to climate changes, ocean eutrophication related to the massive proliferation of land plants, meteorite impacts, global warming, and the greenhouse effect, among other theories [37,38]. In the SPZ, this crisis is manifested by the fragmentation and collapse of the Upper Devonian basin and the subsequent formation of anoxic sub-basins where black shales and, in some cases, massive sulfides were deposited [33]. An environment of high seismic and magmatic activity was widely evidenced in the regional stratigraphic record [39,40]. Seismic activity affected both the IPB and the southwest Portuguese Domain [40], whereas other geological aspects—manifested with intensity in the FPI—affected to a lesser extent the northern Pulo do Lobo Domain. The initial tectonic regime was extensional (transtensive) and involved strong crustal thinning and the rise of deep-seated magmas [41–43]. Data derived from the IBERSEIS seismic profile suggest that the triggering phenomenon of the IPB crisis was related to an intense mantellic activity [44,45]. Also, in the Pulo do Lobo Domain, the magmatic activity was recorded as bundles of mafic dikes with MORB affinity [46] intersecting the Pulo do Lobo Formation. In the absence of geochronological data, the equivalence between the mafic rocks of both domains is here proposed.

The VSC represents the stratigraphic record corresponding to the time when magmatic activity (effusive or subvolcanic) conditioned the dominant geological processes in the region. Its age has been roughly established as between the late Famennian and the middle Visean [16,47–49], although felsic volcanic rocks down to 374 Ma (the late Frasnian) have been recently reported in the western sector of the basin, see [50] and the references therein. Relatively recent palynological studies assign local ages ranging from the Strunian [51] to the late Visean/Moscovian [52,53]. The synchronous/diachronous nature of the top and base of the VSC has been widely debated. Currently, there is a general consensus regarding the diachronous nature of the onset of Culm facies (and therefore the end of the CVS), which progressed from north to south (according to the current position of the Iberian Peninsula) ahead of the orogenic front, see [54,55] and the references therein. Regarding the base of the CVS, the issue remains unresolved, both in terms of age and stratigraphic relationships with the underlying PQ.

Regarding the age, initial models advocated for a S-N migration of the magmatic onset in the IPB [16,27,48,56], SW-NE [57], or even NW-SE [58]. Rosa et al. [59] revisit the topic of the S-N migration using U-Pb dates from magmatic zircons, at various locations in

Portugal, and previously published data in the Spanish part of the IPB. Chronostratigraphic data based on available palynological studies [52,60,61] suggest that regional volcanism occurred in relation to the Late Devonian crisis, so that, although its regional distribution was heterogeneous, the onset of magmatism and subsequent volcanic activity occurred, in a generalized manner, throughout the region, in the late Famennian. From the above, it is inferred that this is an unresolved issue and that detailed studies are needed on both sides of the Spanish–Portuguese border to resolve it.

The stratigraphic relationships between the underlying PQ and the VSC have also been a subject of debate. Most authors consider the PQ-CVS contact as conformable [4,16,22,42,49,62,63]. Others, however, postulate the existence of an angular unconformity between both formations [47,48,64]. The Late Devonian unconformity, as proposed by the French authors in [47,48], would be associated with a bulging of the IPB basin, the most significant effect of which would be the rupture of the basin and the subsequent distribution of volcanic and sedimentary lithofacies, including here the massive sulfides and the manganese jaspers. An argument in favor of this hypothesis is the frequent intrusion of mafic sills at the PQ-VSC contact [48,65] emplaced along the unconformity, according to the cited authors. This is an observation evidenced in maps at scales smaller than 1:50,000; however, at larger scales, it is observed that the mentioned mafic sills intrude near but not necessarily right at the PQ-VSC boundary. For example, in the Jarama stream section, subvolcanic mafic rocks are intercalated within a volcaniclastic sequence, rich in pumice fragments, at the base of the VSC. The authors in [64,66] base their proposal of unconformity on local mapping data, and although these are not discussed in detail, they are represented as a certain fact in their Figure 2.

The unconformity between PQ and VSC cannot be argued as a secure fact for the entire IPB, although the occurrence of some outcrops with high continental influence could indicate punctual emersions and local paraconformity relationships. In general, observations at the outcrop scale in different parts of the basin show a gradual transition between PQ lithofacies and well-stratified volcaniclastic rocks. In other cases, the transition is marked by a sequence of black shales, where bedding surfaces and stratigraphic relationships are obscured by the deformation. In such cases, the existence of an unconformity cannot rigorously be ruled out. However, no single borehole cutting the PQ-VSC transition has provided evidence of the aforementioned unconformity.

From a lithological point of view, the VSC is constituted by a heterogeneous sedimentary series with intercalations of magmatic rocks with differences in texture and compositions (Section 3). Among the sedimentary rocks, the most abundant are the detrital and also the volcaniclastic rocks derived from the erosion and redeposition of non-cohesive volcanic materials. It is also worth noting the common occurrence of chemical sedimentary rocks, among which massive sulfides, manganese jaspers, and some discontinuous lenses of fossiliferous limestone are included. The regional distribution of sequences dominated by magmatic or sedimentary rocks is heterogeneous. Generally, sediment-dominated columns predominate toward the south of the IPB, and magmatic rocks toward the north, with subvolcanic rocks prevailing over volcanics among them.

The lutitic lithofacies consist of dark-colored shales and mudstones with variable organic matter content [67–72]. In some cases, they are pure black shales with organic carbon contents of up to 5%, but in most cases, organic carbon contents are less than 1% [70]. It is notorious that most giant deposits and many medium and small ones feature dark-black shales associated with sulfides [73]. Toward the top of the VSC, there is an oxidized sequence, ranging in color from red to violet and in grain size from clay to fine sand. Its thickness, commonly decametric, occasionally reaches a hundred meters. By contrast, its lateral continuity is significant, as it probably covered most of the IPB at the time of deposition. Local geologists describe them as purple shales, purple tuffs, or purple slates; French authors refer to them as “ardoises violettes”. Despite serving as a key mapping horizon and representing one of the most characteristic lithofacies of the IPB,

in the absence of textural or compositional data to deduce its origin, very little is known about this lithofacies.

Siliceous rocks (chert) are another significant lithology in the IPB. They appear at different levels within the stratigraphic series, and in some cases, they are associated with Mn-rich deposits, exploited by ancient miners. Manganese mining in the IPB began in 1858 [18] and reached its peak at the end of the 19th century. During that time, the province of Huelva became the major Mn producer, supplying almost two-thirds of the world's consumption [2]. Throughout the second half of the 20th century, production gradually declined until the closure of the last mine, Soloviejo, which permanently ceased its operations in 1973. Siliceous rocks appear as discontinuous levels, metric to decametric in thickness. Due to their resistance to weathering, their main outcrops stand out in the regional landscape, forming steeply topographic ridges. Studies conducted to date have primarily focused on evaluating possible geochemical relationships between siliceous rocks and massive sulfides, yet no geochemical pattern has been found linking both lithologies [74].

The volcanoclastic rocks exhibit highly variable grain sizes, ranging from fine sand to boulders. Their composition is similar to that of the exposed volcanic rocks, with a predominance of felsic over mafic components. Most volcanoclastic rocks show low indices of textural maturity (sorting and roundness), suggesting mass transport and little reworking in the deposition area. This general rule is often not observed toward the top of the VSC, where volcanoclastic lithofacies with sand-sized grains that frequently show an internal order appear. These lithofacies were grouped with the basal Culm shales as part of the "Basal Shaly Formation" reported by Moreno and Sequeiros [75].

The Culm Group comprises the post-volcanic sedimentary rocks of the IPB, excluding the molassic Viar Basins (Spain) and Santa Susana Basin (Portugal). It consists of three stratigraphic units named by Moreno [62] and Moreno and González [63] as follows: Basal Shaly Series; Turbiditic Formation of Culm facies; and Shallow Platform Sandy Unit. The Basal Shaly Series is a mixed sequence of volcanoclastic rocks and black shales with abundant Posidonia and goniatite fossils and phosphate-rich concretions. Its thickness reaches 50 m in some areas but it is absent in others. The goniatite remains contained in the shales have provided a late Visean age [76]. The paleogeographic significance and detailed description of this unit are found in the reference work by Moreno and Sequeiros [75]. The Turbiditic Formation of Culm facies is a turbiditic sequence composed of shales, litharenites, and sparse conglomerates, constituting the flysch deposits of the Variscan orogeny in the IPB. Paleocurrents, facies distribution, and petrography of the sandstones suggest both the OMZ and the IPB are source areas for the detritus constituting the sandstone framework [62,77]. Its original thickness has been estimated at several thousand meters, and its age ranges from late Visean to late Moscovian [16,21]. The Shallow Platform Sandy Unit has limited outcrops. It is composed of alternations of shales and quartzose sandstones with typical sedimentary structures of shallow marine environments [62,78]. The Culm Group is referred to by some Portuguese authors as the Baixo Alentejo Flysch Group, being divided into three formations (Mértola, Mira, and Brejeira) based on the type and predominance of turbiditic facies [54].

The stratigraphic relationships between the VSC and the Culm Group are also subject to discussion using the same arguments previously used for PQ-VSC contact. In principle, the geometric relationships suggest concordance at the outcrop scale. From a conceptual point of view, the Culm, representing the flysch facies of the Variscan orogeny, constitutes the infill of the synorogenic basins dominated by a north–south migration of the orogenic front, according to current coordinates. Petrographic study of the Culm sandstones [77] reveals the presence of IPB-derived volcanic and sedimentary rock fragments among the most abundant lithic components of the sandstone framework. This, along with additional sedimentological and paleogeographical data referring to facies distribution and sediment sources, suggests that at least part of the IBP emerged and was subjected to erosion [62]. The onlap of Culm turbidites onto erosive surfaces and their correlative paraconformities would

lead to local unconformities in proximal areas of the basin, as advocated by [49,62,78]; however, no outcrop has been described so far showing such relationships. It is to be assumed that if they existed, they must have been eroded during the mountain uplift associated with orogenic shortening. Other authors, such as [64] (in their Figure 2), also argue for a discordance between both formations, although they do not provide reasons in the text.

3. Magmatism

The massive sulfide deposits of the IPB were formed during a prolonged period of magmatic activity, spanning from approximately 375 Ma (Frasnian) to 330 Ma (Visean), see [50] and the references therein. This magmatic activity produced mafic (dolerites and basalts), intermediate (andesites), and felsic (dacites and rhyolites) volcanic and subvolcanic lithofacies [79–82]. The distribution of these lithofacies, as estimated from a 1:200.000 geological map [83], is 18% basic, 26% intermediate, and 58% acid.

Basic magmatism in the IPB is characterized by the presence of subvolcanic bodies, pillow lavas (Figure 4a), and various types of autoclastic and syn-eruptive resedimented volcaniclastic deposits (se McPhie et al. [84]) [79,80,85]. Intermediate and felsic rocks are observed as sills [85,86], lava/dome complexes associated with in situ and resedimented hyaloclastite (Figure 4b), or pyroclastic deposits [87–91]. Peperites are noted at the contacts of sills or at the base of lava flows (Figure 4c). The volcanic facies architecture and the compositional evolution of magmatism vary across different areas of the IPB. This magmatic activity is commonly interpreted as occurring in multiple basins that evolved from subaerial environments, with pyroclastic deposits (Figure 4d), to deeper submarine settings, where lava flows and domes associated with hyaloclastite deposits and shallow-level subvolcanic sills predominate [42,89,91,92].

Petrographically, mafic igneous rocks exhibit an intergranular to subophitic texture, with fine to very fine grain size, primarily composed of plagioclase and occasionally augite. Some alkaline mafic rocks contain titanian augite phenocrysts. Andesites display a porphyritic texture with abundant medium-grained plagioclase phenocrysts embedded in a groundmass of plagioclase microliths and interstitial chlorite (Figure 4e). Dacites are petrographically similar to andesites but also feature engulfed quartz phenocrysts. Both andesites and dacites can also include augite phenocrysts. Rhyolites are characterized by a porphyritic aphanitic texture with phenocrysts of feldspar and quartz, smaller than those in dacites, and included in a (glassy) quartz-feldspathic microcrystallized groundmass (Figure 4f). The chemical and mineralogical compositions of these rocks are significantly influenced by regional metamorphism and hydrothermal alteration [93], as well as by secondary alteration stages related to massive sulfide mineralization [79,94].

The alteration processes produce loss or gain of mass in these rocks. For this reason, the evaluation of the petrogenetic processes requires the use of elements that remained immobile during alteration [95]. Primitive mantle-normalized immobile element patterns reveal the existence of subalkaline (tholeiitic) and alkaline mafic igneous rocks (Figure 5a) [79,80]. The alkaline mafic rocks are enriched in light rare-earth elements (LREE) relative to heavy rare-earth elements (HREE) and have a slight positive Nb anomaly. The tholeiitic mafic rocks display slight HREE enrichment and a negative Nb anomaly compared to the alkaline rocks (Figure 5b). Rhyolites are characterized by patterns showing high LREE enrichment; pronounced negative Nb, P, Ti, and Eu anomalies; and relatively flat HREE contents. Dacites exhibit similar REE patterns but with smaller negative Nb, P, Ti, and Eu anomalies compared to most rhyolites (Figure 5c). Andesites also present similar patterns but have the smallest negative anomalies in these elements (Figure 5b) [79,80,96]. Despite their close spatial and temporal association, geochemical and isotopic data exclude any relationship by fractional crystallization between mafic, intermediate, and felsic rocks [79,80,97].

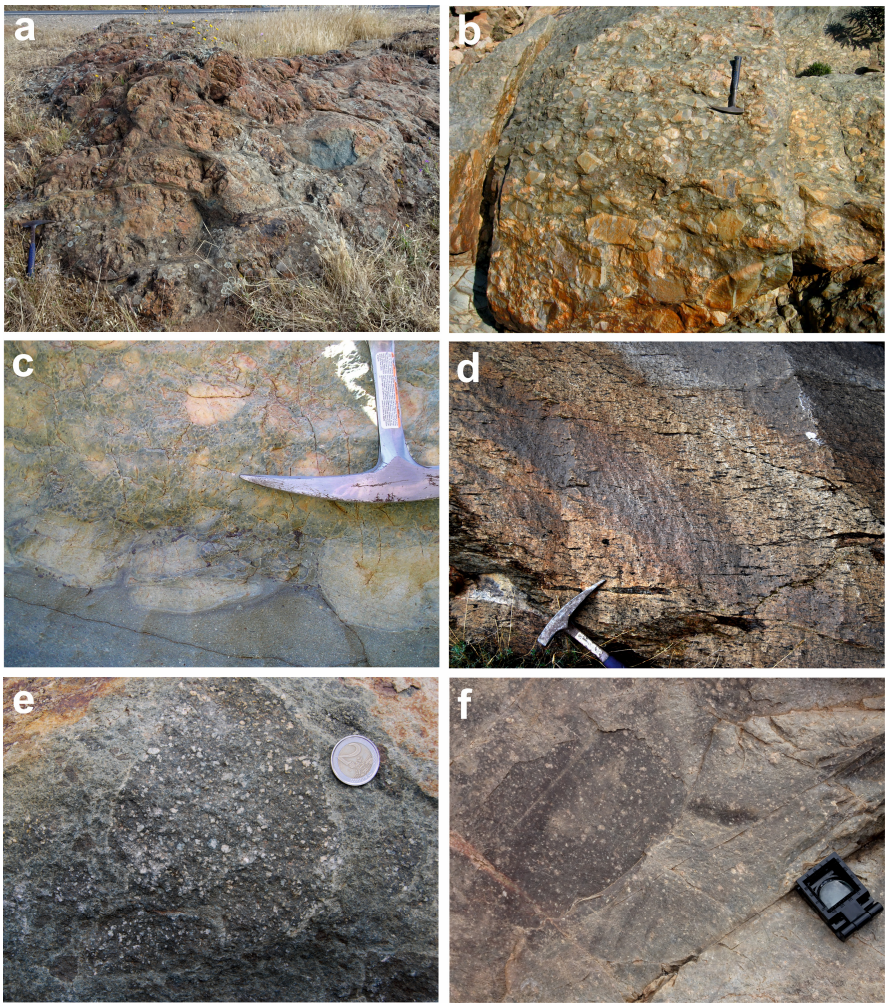

Figure 4. Field features of igneous rocks in the IPB. (**a**) Closely packed basic pillow lavas; (**b**) resedimented hyaloclastite breccia; (**c**) peperite at the lower contact of a rhyolitic lava flow with a volcanic sandstone; (**d**) eutaxitic texture in a welded ignimbrite containing "fiammes"; (**e**) highly plagioclase–phyritic andesite; (**f**) quartz–feldspar–phyric rhyolite.

Although commonly considered a bimodal magmatism [1,48,79–81,98,99], the significant presence of andesites [100] has sparked debate about the geotectonic context of the IPB. Basic magmatism is considered tholeiitic with chemical traits transitional to arc tholeiites [79], continental tholeiites [80,81], arc-related basalts [81], and calc-alkaline rocks with variable to no contamination from crustal material [97]. In contrast, the alkaline mafic rocks are comparable to recent within-plate alkaline basalts [79–81]. It is postulated that mafic rocks originated initially as either a series of partial melts from a heterogeneous peridotitic mantle at various depths and degrees of melting [79] through a single mixing model between E-MORB and N-MORB with assimilation of crustal material [80], or by melting of a spinel–lherzolite mantle source for tholeiitic rocks and a garnet–lherzolite source for the alkaline rocks [97].

The diversity of chemical and Sr–Nd isotopic composition, along with the significant proportion of inherited zircons (Proterozoic to Devonian) in felsic rocks, can be attributed to the partial melting of a heterogeneous crustal source [79–81,101] containing older detrital components [59,102]. The LREE/HREE ratio and the negative Eu anomaly indicate the presence of feldspars (plagioclase and/or alkali feldspar) and a ferromagnesian phase (amphibole or pyroxene), and the absence of garnet in the source area. Consequently, partial melting of an amphibolite within the middle to lower continental crust is commonly proposed [79,80,96,97,103,104]. The presence of peritectic garnet in some felsic rocks also

suggests partial melting of biotite-bearing metapelites [105]. This acid magmatism was likely driven by heat supplied by rising mafic magmas [59,79–81]. Andesites have been interpreted as resulting from partial melting of the mantle [79] or from contamination/mixing between basaltic magmas and upper crustal material [80,103,106].

In the IPB, two significant mineralization events have been identified: (1) at the Famenian–Tournaisian boundary; (2) near the Tournaisian–Visean boundary (see below). During the first event, sulfide deposits are associated with black shales or black shales and coeval rhyolitic rocks [101,107], while in the latter, they appear at the top of coherent rhyolitic facies. Despite the abundance of felsic igneous rock types, those associated with massive sulfide deposits exhibit distinct geochemical and isotopic characteristics [82,103,104,108]. However, the emplacement depth of these rocks is also considered a critical factor in explaining the presence of such deposits.

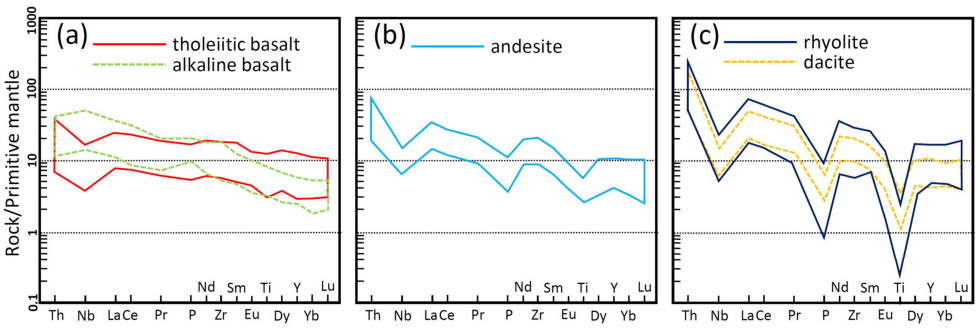

Figure 5. Primitive mantle's normalized [109] immobile element patterns for igneous units within the IPB: (**a**) mafic rocks; (**b**) andesites; (**c**) felsic rocks. Chemical data are from [82,83,91,104].

4. Deformation and Metamorphism

The rocks of the SPZ were deformed and slightly metamorphosed during the Asturian Phase of the Variscan orogeny. The manifestations of this orogeny vary in age and intensity due to the migration of the orogenic front from north to south, according to present-day coordinates [16,55,110]. The oldest deformation ages correspond to the middle-upper Visean (342 Ma) and have been determined using $^{40}Ar/^{39}Ar$ dating in the Beja amphibolites [111], which overthrust the SPZ via a ductile shear with left oblique thrust kinematics [55,112]. The orogenic front reached southwest Portugal in the Moscovian [16,49].

The deformation presents a general tectonic model of the "thin-skinned" type [113,114], characterized by a main system of thrusts rooted in the middle crust [44]. Near the boundary with the OMZ, the deformation is intense, resulting in complex structures; toward the south, these structures gradually simplify. The dominant vergence of the main structures is toward the south, and the associated foliation presents a direction that evolves from NW-SE at the NW end of the SPZ to E-W in the easternmost outcrops located north of Seville. The general dip is toward the north and ranges around values close to 70°.

5. Geodynamic Setting

Despite the extensive geological research on the IPB, its geodynamic evolution remains a subject of debate [16,79,80,100,109,115–117]. Most geodynamic models propose an oblique subduction and subsequent collision of two continental plates during the Variscan orogeny [44,49,64,113]. This collision, which is diachronous within the Variscan orogen, occurred between 340 and 335 Ma in southwest Iberia, involving left-lateral transpressional kinematics [44,49,64]. In this context, geodynamic models differ in the plate where magmatism occurs, distinguishing two main groups: those that locate the IPB magmatism in the continental crust of the subducting tectonic plate, and those that place it overriding the continental tectonic plate.

In the first scenario, magmatism in the IPB would develop in a series of pull-apart continental-to-marine basins formed during the left-lateral transcurrent faulting generated

by the oblique subduction [16,49,113,118]. During this process, rapid decompression caused by lithospheric thinning [80], lithospheric mantle foundering and delamination [117], or the involvement of a deeper mantle [44,50] could be the triggering mechanisms for asthenospheric melts.

In the second scenario, the IPB magmatism is considered to have occurred under various geodynamic contexts: (a) in an active continental margin evolving into the initial stages of the opening of an ensialic back-arc basin [79]; (b) in a volcanic arc associated with two separate northward-dipping subduction zones [100]; (c) in a forearc basin over an accreted crustal segment [81]; or (d) through asthenospheric upwelling related to slab break-off in response to the Neo-Acadian collision between Meguma and Avalonia (Laurussia), soon followed by an intracontinental extensional setting as a result of the Variscan collision between Gondwana and Meguma (Laurussia) [97].

6. IPB Metallogeny

The IPB is characterized by its significant metallogenic productivity, to the extent that it is considered one of the largest massive sulfide reserves in the world. In addition to massive sulfide deposits, the region has an abundance of stratiform Mn-rich deposits [1,2,22,48,119] and vein-type mineralizations, most of which are related to the late- and post-Variscan evolution of the region [120–124]. The vein-type deposits include base metal mineralizations (Cu, Pb, and Zn), as well as Ni-Co, Sb, As, F, Ba, and Sn-W. Generally, they are smaller than the massive sulfide deposits, although they have played an important role as a metal source in prehistoric times and at the onset of metallurgy in the southwestern part of the Iberian Peninsula [125,126].

6.1. Massive Sulfides

Massive sulfides of the IPB generally appear as stratiform deposits concordant with the host rocks and, occasionally, exhibit more complex geometric relationships due to replacement. They are primarily composed of pyrite with minor amounts of base metal sulfides (chalcopyrite, sphalerite, and galena). The grain size is generally fine, and poikiloblastic textures are abundant. Historically, this has complicated the mineral separation processes, leading mining activities to focus mainly on the exploitation of pyrite for sulfuric acid production and Cu leaching from the roasting ashes. Technological advancements since the second half of the 20th century have enabled the application of efficient grinding and flotation techniques for the differential concentrations of various metals. Recently, a patent was registered under the acronym E-LYX for a system designed for the direct production of Cu cathodes at Riotinto Mine. This kind of technology could open new perspectives for the exploitation of texturally complex sulfide deposits, such as those from the IPB. Currently, this region is one of the most significant metallogenic provinces for the production of base and precious metals in Europe.

In addition to these resources, some deposits rich in Sn have been exploited, including Neves-Corvo. Anomalous Sn contents have been identified in potentially economic quantities in recent exploration projects, such as those by Panglobal Resources near the historic district of Aznalcóllar, and in some intersections reported by Emerita Resources in Romanera. The potential for the IPB as a source of strategic metals (e.g., Co in Tharsis [127]; In and Se in Neves-Corvo [128]) remains to be defined.

At a regional scale, the location of massive sulfide deposits and occurrences appears to follow a banded distribution generally aligned with major regional Variscan structures [14,42,48,129], as shown in Figures 1 and 6. Such distribution may be related to the original paleogeography of the Devonian-Carboniferous IPB basin, controlled by E-W and NE-SW fractures [33,42,62].

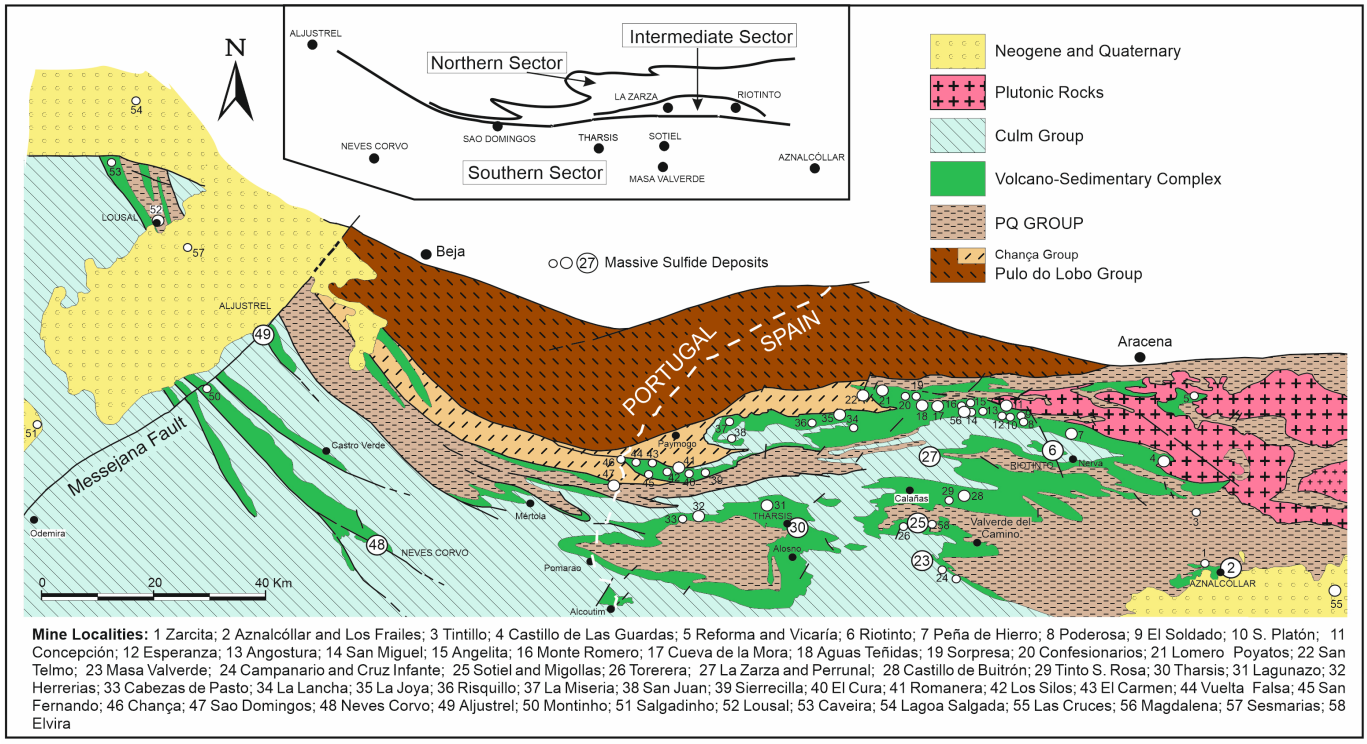

Mine Localities: 1 Zarcita; 2 Aznalcóllar and Los Frailes; 3 Tintillo; 4 Castillo de Las Guardas; 5 Reforma and Vicaría; 6 Riotinto; 7 Peña de Hierro; 8 Poderosa; 9 El Soldado; 10 S. Platón; 11 Concepción; 12 Esperanza; 13 Angostura; 14 San Miguel; 15 Angelita; 16 Monte Romero; 17 Cueva de la Mora; 18 Aguas Teñidas; 19 Sorpresa; 20 Confesionarios; 21 Lomero Poyatos; 22 San Telmo; 23 Masa Valverde; 24 Campanario and Cruz Infante; 25 Sotiel and Migollas; 26 Torerera; 27 La Zarza and Perrunal; 28 Castillo de Buitrón; 29 Tinto S. Rosa; 30 Tharsis; 31 Lagunazo; 32 Herrerias; 33 Cabezas de Pasto; 34 La Lancha; 35 La Joya; 36 Risquillo; 37 La Miseria; 38 San Juan; 39 Sierrecilla; 40 El Cura; 41 Romanera; 42 Los Silos; 43 El Carmen; 44 Vuelta Falsa; 45 San Fernando; 46 Chança; 47 Sao Domingos; 48 Neves Corvo; 49 Aljustrel; 50 Montinho; 51 Salgadinho; 52 Lousal; 53 Caveira; 54 Lagoa Salgada; 55 Las Cruces; 56 Magdalena; 57 Sesmarias; 58 Elvira

Figure 6. Geological map of the IPB showing the division into bands that group deposits with equivalent characteristics and the location of the main deposits exploited along the mining history of the region. Modified from [4].

The northern band exhibits an exceptionally high concentration of medium to small-sized sulfide deposits (1–50 Mt), generally associated with felsic volcanic rocks. They are rich in base metals (Cu, Zn, and Pb) and precious metals (Au and Ag). Within this band, between the meridians of Peña de Hierro and the Portuguese border, an area of approximately 300 km^2 hosts around 30 mines, indicating that there is an economic deposit roughly every 10 km^2.

The southern band is characterized by a much lower concentration of ore deposits. They are significantly larger and are preferentially associated with black shales. In terms of metal content, they range from base-metal-rich deposits, such as Neves-Corvo, Sotiel-Migollas, or Aznalcóllar-Los Frailes, to essentially pyritic deposits like Tharsis. This band hosts five of the eight supergiant (>100 Mt) massive sulfide deposits identified to date in the IPB (see Figure 6). The central band is more heterogeneous and includes giant deposits such as Riotinto, La Zarza, and possibly Aljustrel, along with several other smaller deposits. These deposits are associated with both volcanic and sedimentary rocks and their metal contents vary from one case to another.

Examining the metallogenic province as a whole, a heterogeneous distribution of massive sulfide deposits is observed. The density of deposits in the Spanish part of the IPB is significantly higher than in the Portuguese counterpart (Figures 1 and 6). The obvious reason is that the proportion of VSC outcrops, the lithostratigraphic unit hosting the deposits, is much smaller in Portugal. There, this unit is mostly covered by rocks of the overlying Culm Group or by the Sado Basin cover deposits. Considering that there are no known paleogeographic reasons controlling the decrease in massive sulfide deposits toward the west of the IPB, the gradual improvement of exploration methods, associated with technological innovations, should open new perspectives for the future of mining in the region.

Despite the intense tectonic deformation affecting the IPB, the massive sulfide deposits relatively conform well to the conventional model of exhalative sulfide deposits: lenticular or tabular masses of massive sulfides, essentially concordant with stratification, positioned

above disseminated or stockwork mineralization. This arrangement is often modified by Variscan deformation, with several cases described where stockwork-type mineralization has been thrust over the massive sulfide mineralization. This model has been described at Aznalcóllar [41], Neves-Corvo [130], and Sotiel-Migollas [131], and also appears to be the structure of the La Zarza deposit [132].

Most of the giant deposits are composed of several massive sulfide bodies located at the same stratigraphic level (see Table 3 in [129]). An exception to this rule is La Zarza, where a single massive body totals more than 100 Mt of massive sulfides (Strauss et al. [132] reported 161 Mt at 1.24% Cu, 1.9% Pb, 2.9% Zn, 47 g/t Ag, and 1.79 g/t Au).

6.2. Relation with the Hosting Rocks

From a stratigraphic perspective, the IPB massive sulfides are associated with black shales and felsic volcanic rocks, with no known cases of association with mafic rocks. Toward the top, the presence of siliceous rocks is common, although only exceptionally (e.g., Aljustrel and Magdalena) are they in direct contact with the massive sulfides [74,133–135]. The schematic N-S profile in Figure 7 illustrates the nature of the sulfide deposit host rocks according to their location within the metallogenic province.

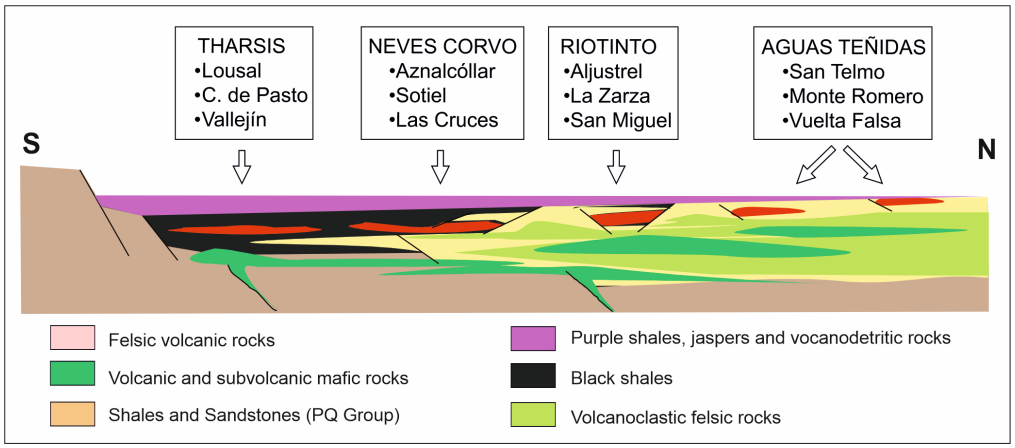

Figure 7. Idealized N-S profile indicating the position and nature of the hosting rocks and substrate of the sulfide deposits according to their location.

Black shales occur as the dominant lithofacies in relation to the massive sulfides, as observed in Tharsis [22,136,137], Lousal [22,138], Sotiel-Coronada [131,139], Aznalcóllar [41], Masa Valverde [140], and Herrerías [141], or as a subordinate lithofacies, as in San Miguel [11], Riotinto [142], La Zarza [132], Neves-Corvo [92,130], Las Cruces [143], and Torerera [141]. The replacement of black shales by massive sulfides is a relatively common process [135].

When massive sulfides are hosted by volcanoclastic rocks, these are felsic and generally fine-grained. In exceptional cases, massive silfides are directly deposited on coherent rocks (e.g., some deposits in the Riotinto district or the central part of the San Miguel deposit). In these cases, a continuous transition occurs from stockwork-type mineralization to massive sulfide, with a gradual increase in the vein/host rock ratio, leading to the replacement of volcanic rock by massive sulfides [115]. A similar process has been described for coarse-grained volcanoclastic rocks with high primary porosity [129,135].

6.3. Mineralogy and Zonation

The mineralogical composition of massive sulfides and stockworks is qualitatively similar in terms of ore mineralogy. In both types, the dominant sulfide mineral is pyrite. Subordinate phases include sphalerite, galena, chalcopyrite, and tetrahedrite. A large number of minor minerals have been described, including pyrrhotite, marcasite, arsenopyrite, stannite, Cu-Pb and Bi-Pb sulfosalts, bismuthinite, cobaltite, barite, siderite, ankerite, cassiterite, magnetite, hematite, bismuth, gold, and electrum [22,41,48,135,144–147]. Based on

the relative proportions of the major phases, three major types of mineralizations have been distinguished, referred to as follows: pyritic, cupriferous, and polymetallic. The special case of Neves-Corvo also includes tin-rich ores as a metal type. Ore mineral distribution within the deposits usually follows common zonation patterns of massive sulfides, although in many cases, the original arrangement of the types of mineralization has been modified by the Variscan deformation and associated remobilizations (Figure 8).

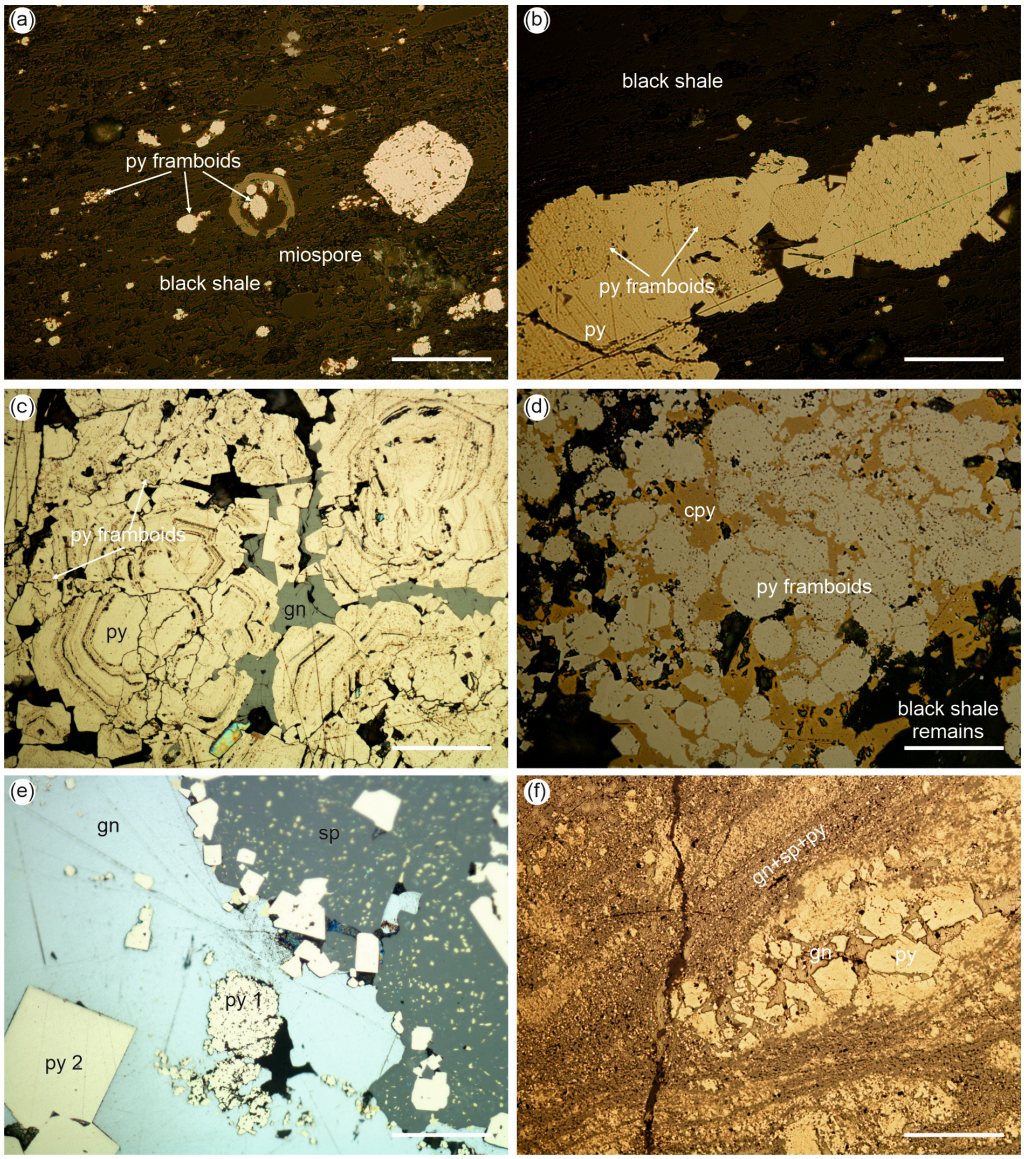

Figure 8. (**a**) Framboidal and diagenetic cube-shaped pyrite disseminated in black shale. Vitrinite miospore partially corroded during BSR activity. Scale bar 50 microns; (**b**) coalescence and recrystallization of framboidal pyrite in black shales. Scale bar 50 microns; (**c**) collophorm pyrite (py) growing after early framboids. Late galena (gn) fill voids and corrode early pyrite. Scale bar 100 microns; (**d**) late chalcopyrite (cpy) growing over early framboidal pyrite. Scale bar 50 microns; (**e**) late stage of mineralogical and textural evolution during massive sulfide genesis. Early and recrystallized pyrite (py 1 and py 2, respectively) included in galena (gn) and sphalerite (sp), which also show chalcopyrite disease. Scale bar 100 microns; (**f**) tectonic fabric produced in massive sulfide ore by unusual behavior of sulfide minerals. Pyrite porphyroclasts are surrounded by a fine-grained groundmass made by galena (gn), sphalerite (sp), and pyrite. Fractures generated due to brittle behavior of pyrite are filled by galena. This pattern resembles common protomylonitic textures. Scale bar 50 microns.

Generally, the cupriferous facies are preferentially related to the stockworks and the central-lower parts of the massive sulfide bodies. Polymetallic facies are typically located at the top and lateral zones of the deposits, while pyrite-rich mineralizations, with low base-metal content, usually constitute the main body of the massive sulfides and part of the stockwork. Examples of zoning according to this description include the ore deposits of Monte Romero [148] and Feitais in Aljustrel [149]. However, this general model is not always followed. In the IPB, there are frequent occurrences of pyrite-rich mineralizations without associated cupriferous or polymetallic facies. Filón Norte, in the Tharsis mining district, serves as an example [22]. Pyrite—along with other sulfides to a lesser extent—also appears as disseminations in the vicinity of veins or more generally in the altered rocks at the footwall of the massive sulfides. In most stockworks, these disseminations consist primarily of pyrite. However, there are exceptional cases where base metal sulfides are disseminated within the stockworks. One such example is the mineralization locally referred to as "pyroclast," which was exploited in Aznalcóllar for its copper content, or the mineralization at Monte Romero, exploited by Asturiana de Zinc for the production of Cu, Pb, and Zn concentrates. Additionally, there are base-metal-rich mineralizations with no apparent relationship to significant masses of sterile pyrite, as seen in the Sierrecilla deposit [150].

Textural analysis of the massive sulfides reveals complex relationships dominated by recrystallization and deformation textures over primary textures, both in massive sulfides (Figures 8 and 9) and the stockworks (Figure 10). Excluding textural features related to the Variscan deformation, a general progression can be observed from framboidal and colloform textures (Figure 8a,b) to more mature textural forms characterized by widespread recrystallization and replacement of primary phases (Figure 8d,e) [135,151]. Variscan deformation results in cataclastic textures, mainly in pyrite, and banded textures where ductile deformation and the flow of sphalerite, chalcopyrite, and galena produce mylonite-like microstructural patterns (Figure 8f).

Process	Texture	Temperature	Geochemistry/ Mineralogy
Primary textures associated with exhalative-sedimentary and diagenetic processes	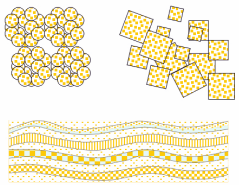	< 200 ºC	**S + Fe (Pb+Zn+As)** --- **py** ± mc, ga, sph, apy, cpy, monosulf
Recrystallization and hydrothermal replacement	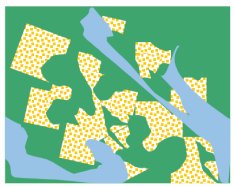	250 – 400 ºC	**Fe+Zn+Pb+Cu** ± (As, Sb, Sn, Co, Bi...) --- **py + sph + cp + ga +** po, tt, apy, st, stn, bar, boul, bour, co, Bi, Au...
Tectonic and/or metamorphic remobilization	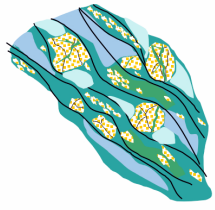	200 – 300 ºC	**Sb** ± (Fe, Zn, Pb, Cu) (As, Sb, Sn, Co, Bi...) --- **cpy + sph + ga** + tt (apy, boul, bour, Au)

Figure 9. Mineralogy and main textural features of the massive sulfides from the IPB. (py: pyrite; mc: marcasite; ga: galena; sph: sphalerite; apy: arsenopyrite; cpy: chalcopyrite; po: pyrrhotite; tt: tetrahedrite–tennantite; st: stannite; stn: stannoidite; bar: barite; boul: boulangerite; bour: bournonite; co: cobaltite; Bi: bismuth; Au: gold.)

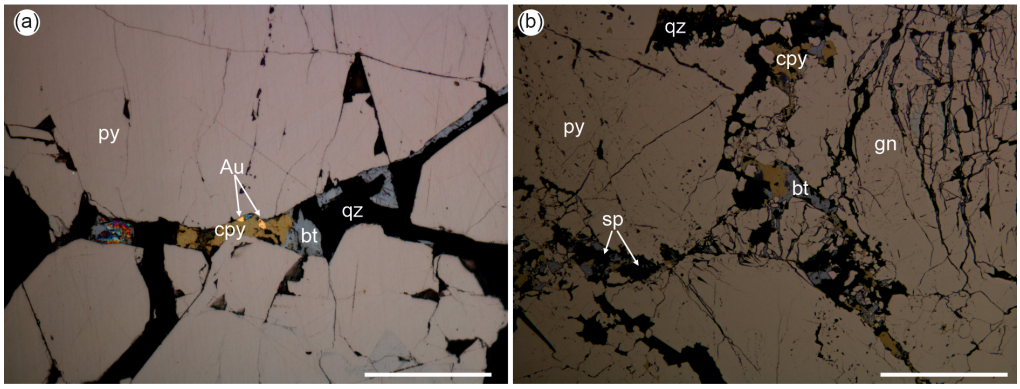

Figure 10. (**a**) Free gold together with pyrite (py), calcopyrite (cpy), and bismuthinite (bt) in a quartz (qz) vein from San Guillermo stockwork (Tharsis district). Scale bar 50 microns; (**b**) cataclastic texture in stockwork vein from San Guillermo orebody (Tharsis district). Interstitial galena (gn) and sphalerite (sp) fill voids in fractured pyrite, chalcopyrite (cpy), and bismuthinite (bt) also mobilized during deformation. Scale bar 50 microns.

Stockwork mineralization consists of a network of veins that are essentially composed of pyrite, chlorite, and quartz. Other sulfides, including chalcopyrite, galena, sphalerite, arsenopyrite, cobaltite, bismuthinite, and Pb-Bi and Cu-Pb sulfosalts occur in smaller amounts. Carbonates (ankerite and siderite), occasional oxides (magnetite and cassiterite), and precious metals (gold, electrum, and Au-Ag-Hg amalgams) are also present (Figure 10a). The grain size of the crystals is larger than in massive sulfides. Pyrite tends to form idiomorphic or subidiomorphic crystals that are often fractured and cemented by chalcopyrite and, occasionally, by other sulfides or sulfosalts (sphalerite, galena, or tetrahedrite) or by quartz and/or carbonates. The resulting texture exhibits cataclastic features similar to those developed in massive sulfides (Figure 10b). Sphalerite, galena, and chalcopyrite are usually interstitial, and in the case of sphalerite, chalcopyrite exsolutions (chalcopyrite disease) are very common.

Microtextural analysis of pyrite using high-resolution techniques (FE-SEM; EPMA; EBSD; LA-ICP-MS; HR-TEM-STEM; TEM_EDS) [127,152] has revealed the existence of nano-zonations determined by the As content and, in some cases, by Co within the pyrite lattice. These studies also show the presence of micron-sized nanoparticles of economically significant metallic minerals (e.g., tetrahedrite, galena, chalcopyrite, cobaltite, gold, and electrum). This research opens new perspectives regarding the mechanisms of metal transport and provides new insights into the relationships between the evolution of massive sulfide-generating systems and the textural evolution of pyrite in both massive and stockwork mineralizations.

6.4. Hydrothermal Alteration

Figure 11 represents the spatial distribution of the hydrothermal alteration in the IPB. This alteration affects rocks from the PQ and CVS units and occurs in two distinct contexts:

1. On a regional scale, most rocks are affected by low-temperature hydrothermal alterations, with the most evident features being the widespread albitization of feldspars and the partial destruction of ferromagnesian minerals. This type of alteration has been termed "hydrothermal metamorphism" [93] or "regional alteration" [4,153]. The extensive volume of affected rocks and the homogeneity of the processes involved indicate the necessity for an immense amount of fluids to generalize the process. Isotopic data (δD; $\delta^{18}O$) [93,154] suggest that the primary chemical agent was seawater with very high fluid/rock ratios. In mafic rocks, regional alteration involves the albitization of plagioclases and the hydration of ferromagnesian minerals, forming amphibole (actinolite) and chlorite. Calcium derived from plagioclase alteration is fixed in the form of epidote, pumpellyite, and carbonates. In felsic rocks, the

most evident feature of regional alteration is the widespread albitization of feldspars, typically accompanied by sericitization, slight chloritization, and in some cases, adularization [42]. Rocks of the underlying sequence (PQ Group) are also affected by regional alteration, with the most evident effects being enrichment in K and significant loss of Na+Ca [155]. These processes involve intense water–rock interactions, with seawater playing a significant role as basin fluids, potentially contributing to the pre-concentration of metals involved in the genesis of the IPB massive sulfides;

2. On a local scale, intense hydrothermal alteration halos develop in the footwall of massive sulfide orebodies. The most characteristic features of these halos are the widespread chloritization and/or sericitization of the rocks [4,42,48,142,156–161]. Additionally, silicification and carbonatization of the rocks are common, often occurring in association with these processes [157,162]. Sericite alteration is typically associated with the initial stages of the hydrothermal system, located in the outer zones and related to relatively low-temperature fluids. The transition from sericite to regional alteration is gradual, often making it difficult to delineate the boundary between the two types. Geochemically, this implies a generalized loss of Na+Ca and a relative gain of K+Al [161]. Chlorite alteration is associated with the core of hydrothermal systems and related to later and higher-temperature processes [41,42,163]. The chlorite associated with the alteration zone is classified within the range of clinochlore, with its composition in terms of Fe/Fe+Mg and Si/Al varying among deposits and from the periphery to the core of the alteration halos [41,160,161,164]. The dioctahedral mica present in the inner alteration halo has a muscovite composition and anomalously high Ba contents [41,157]. Carbonate alteration is evidenced by the presence of Fe-carbonates (e.g., siderite, Fe–dolomite–ankerite), which appear as very thin veins or are pervasively disseminated in the altered rocks. When disseminated, the dominant textural feature is nodules nucleating on chlorite or pyrite. Compositionally, they are characterized by Fe/Fe+Mg ratios between 0.7 and 0.9, with increasing Fe content toward the core of the hydrothermal system. Isotopic ratios ($\delta^{18}O$, $\delta^{13}C$) suggest a hydrothermal fluid derived from modified seawater with a minor contribution of C from the mineralization of organic matter contained in the black shales hosting the studied ore deposits [157,165]. This type of carbonate alteration has been explained in relation to partial boiling processes of the hydrothermal fluids due to decompression during ascent to the seafloor [165]. Silica alteration has been associated with two types of processes. The first involves low-temperature fluids, which leach silica to be deposited in the upper parts of hydrothermal systems, creating siliceous levels through the replacement of shales or volcanic rocks, or by direct deposition on the seafloor [42,74,133,134]. The second involves high-temperature processes associated with the core of hydrothermal systems [41,132]. In some cases, the silicified core of the hydrothermal system is enriched in gold and silver, as occurs in the siliceous mineralization at La Zarza [132,166]. Geochemically, the intensity of the alteration is indicated by the enrichment in Fe+Mg and the loss of Na+K toward the interior of the alteration halo [160]. Some authors have proposed using the Fe/(Fe+Mg) ratio in chlorite and the (Ba+K)/Na ratio in muscovite (sericite) as criteria for evaluating the intensity of the alteration and as vectors for guiding mineral exploration [1,161]. Mineralogically, the neoformation and recrystallization of zircon strongly enriched in rare-earth elements (REE) are characteristic of the inner zone of the alteration halo [167,168].

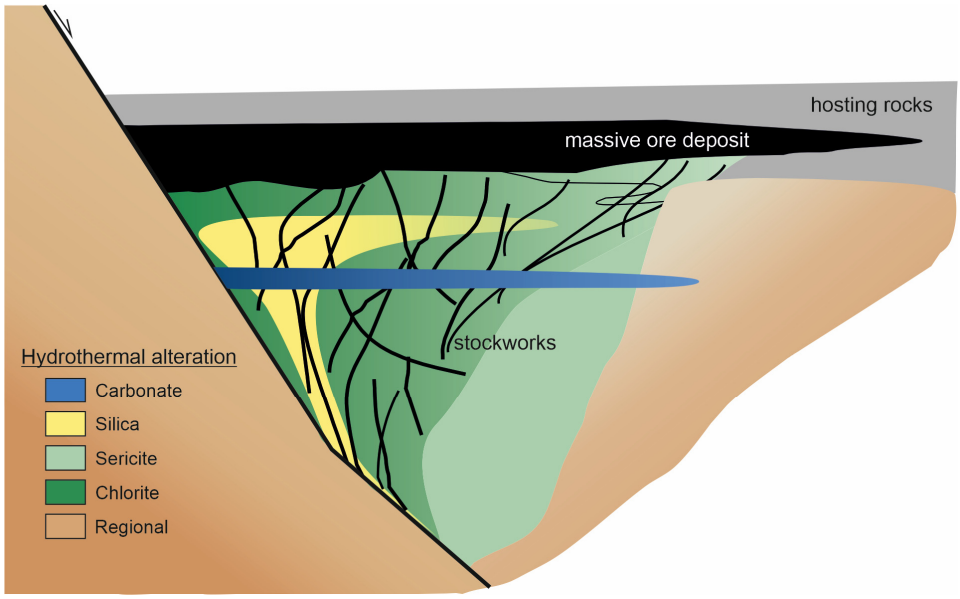

Figure 11. Schematic distribution of different types of alteration in relation to the position of massive sulfides (in black) and stockworks.

6.5. Supergene Alteration

Massive sulfide and stockwork mineralizations exposed at the surface commonly undergo weathering processes, leading to supergene enrichment in Au-Ag within the gossan cap, and Cu in the redox transition zone [169,170]. In the IPB, the resulting mineralizations have been exploited since the dawn of metallurgy in prehistoric times [126]. In recent times, these types of mineralizations have yielded significant Au-Ag [171] and Cu [172] resources. The internal structure of the alteration profile in the IPB mineralizations has been well-described in recent works [173,174]. The upper zone is primarily composed of Fe oxyhydroxides (goethite and hematite) and barite, with Au enrichment due to mass loss. The intermediate zone exhibits complex mineralogy with an abundance of sulfates and sulfoarsenates from the jarosite family (jarosite, natrojarosite, Pb-jarosite, Ag-jarosite, and beudantite) with Au and Ag enrichment. The redox transition from the vadose zone to the saturated zone involves the precipitation of Cu dissolved in percolating waters and significant enrichment of this element in the form of sulfides (chalcocite and covellite) and oxides (cuprite and tenorite). This zone is not extensively represented in many of the IPB deposits [174], although in some (e.g., Riotinto, Las Cruces) it has been of great economic importance. In districts with a less extensive mining history, the existence of gossans has been used as a guide in mineral exploration programs [175]. The long mining history of the IPB [2] means that any surface evidence has already been thoroughly examined, so only those covered by recent sediments (e.g., Las Cruces, Lagoa Salgada) have been preserved to the present day [172,176].

6.6. Mineralogenesis

Currently, there is a general consensus that relates the genesis of the IPB massive sulfides to submarine exhalative processes, in which the stockworks represent the channels for the ascent of hydrothermal fluids [1,4,11–13,42,48,86,129,162,177–179]. This general model shares common features with many of those proposed for the genesis of massive sulfides in various locations around the globe, including the current deposits on the ocean floor [8–10,180–187]. However, discrepancies arise when establishing specific genetic models based on the physicochemical and paleogeographic aspects that influence the genesis and preservation of the IPB massive sulfide deposits.

6.7. Classification

To define the mineralogenetic characteristics of a deposit, it is useful to establish reference models to determine similarities and differences. On a global scale, massive sulfides are traditionally grouped into two major categories—volcanogenic massive sulfides (VMS) and sedimentary exhalative (SEDEX)—although the boundaries between both categories are not precisely defined and hybrid models between the two types can occur in certain geological contexts [8].

The ultimate classification criteria are based on the presence or absence of a genetic relationship with contemporaneous volcanism, and particularly on the characteristics of the involved hydrothermal fluids. Those responsible for the genesis of VMS deposits are composed of seawater injected into convective cells, where it is heated and modified through interactions with volcanic rocks, generally admitting the possible, albeit limited, participation of fluids of magmatic origin. In the case of SEDEX deposits, hydrothermal activity is related to basin fluids mobilized in anomalous geothermal environments where, if contemporaneous magmatism exists, its role is limited to that of the thermal driver of the system.

Chemically, the major difference lies in that fluids related to VMS deposits transport sulfur and metals, subsequently deposited on the seafloor, whereas SEDEX-related fluids transport only metals and require an additional source of reduced sulfur, generally associated with biogenic processes (BSR: bacterial sulfate reduction).

Considering only VMS deposits, the current trend for classification is to use the composition of the host rocks as the discriminating criterion. Based on this criterion, the IPB massive sulfides have been classified as bimodal–siliciclastic-type VMS [187] or the siliciclastic–felsic type [8]. The standard for siliciclastic–felsic VMS deposits would be volcanogenic massive sulfide mineralizations hosted in sequences composed of ~80% felsic volcaniclastic rocks with some lavas and domes and their equivalent intrusive forms, and the rest (~20%) comprising mafic rocks (tholeiitic to alkaline) composed of lavas, sills, and some volcaniclastic materials (~10%), typically located in the capping sequence. Lutite sedimentary rocks and chemical sediments rich in Fe, Mn, Ca, and Ba would also be part of the capping sequence.

It is evident that any resemblance to the sequences hosting the IPB massive sulfides is merely coincidental, and the classification of the IPB within the "felsic–siliciclastic" provinces [8] is imprecise. Barrie and Hannington's [187] proposal is to classify the IPB within the "bimodal–siliciclastic" group. Such a bimodal–siliciclastic type is characterized by similar proportions of volcanic and siliciclastic rocks, with felsic volcanic rocks being more abundant than mafic ones. The felsic rocks are of calc-alkaline nature, while the mafic ones range from tholeiitic to subalkaline. Most deposits are Phanerozoic, and their average size is larger compared to other types. Generally, they are the poorest in Cu and the richest in Pb among the five types of VMS considered by [187]. However, assignment to this bimodal–siliciclastic group fails when examined district by district. The reason lies in the great diversity of types present within the IPB.

Considering the nature of the host rocks as criteria, two subtypes can be distinguished in the IPB, both representing the extremes of a range of intermediate cases. The two subtypes are as follows: (i) deposits predominantly associated with black shales with little or no presence of volcanic rocks (e.g., Tharsis and Lousal); (ii) deposits hosted by volcanic rocks with little or no presence of black shales (e.g., Sierrecilla, San Platón, Aguas Teñidas, and Magdalena).

The distribution of these subtypes appears to be conditioned by paleogeographic factors. When considering an approximate N-S section (Figure 7), there is a predominance of black shales as the hosting rock for the sulfide deposits in the southern part of the province. Toward the north, coherent or felsic volcaniclastic lithofacies constitute the major host rocks, although in many cases, black shales are also observed as a subordinate lithology (e.g., Concepción, Cueva de la Mora, and Peña del Hierro).

6.8. Age of Sulfide Deposits

Radiometric dating of metallic mineralizations using conventional methods (e.g., U-Th-Pb, Sm-Nd, and Rb-Sr) presents some difficulties due to the absence of suitable mineral phases in many cases. The Re/Os system is considered one of the best methods for direct dating since the siderophile and chalcophile nature of these metals facilitates their incorporation into the crystal structure of sulfides and oxides [188,189]; however, its application is limited due to the analytical challenges involved. In the case of the IPB, the ages obtained using the Re-Os system [189–191] coincide, within error margins, with those derived from chronostratigraphic studies, although in most cases, these error margins appear too broad. Additionally, massive sulfides from the Aznalcóllar—Los Frailes district have been directly dated using the U-Th-Pb system on zircons overgrown during hydrothermal alteration [167]. The results, in this case (347 ± 4.7 Ma), do not align well with palynological studies dating the host black shales to the Strunian [192]. Lastly, dating using U-Pb in cassiterite [193] offers a new tool for direct dating, although its application is limited to mineralizations with relatively coarse-grained cassiterite, restricting it so far to the tin mineralization of Neves-Corvo.

Indirectly, radiometric methods (U-Th-Pb system) using magmatic zircons contained in the host rocks have been applied. Dating zircons from the footwall rocks affected by hydrothermal alteration provides a minimum age for the mineralizations but not their absolute age. Another frequently used indirect dating method in the IPB is chronostratigraphy, based on palynological analysis of the black shales associated with many deposits, see [15,137,139,192,194] and the references therein. Although this biostratigraphic tool is certainly accurate, evidence of replacement processes in the black shales during the genesis of massive sulfides [135] introduces some uncertainty in the age assignment. Despite these limitations, published chronostratigraphic and geochronological results [53,102,137,181,189,192,195,196] suggest two massive sulfide mineralization events in the IPB: one at the latest Devonian, in the vicinity of the Devonian–Carboniferous boundary, and another around the Tournaisian–Visean boundary.

Generally, the black shales hosting sulfide deposits in the southern band contain palynological assemblages [137,139,192,194] assigned to the LN biozone of the Western Europe biozonal scheme by Streel et al. [197]. Available geochronological results [98,180,182,188] are also compatible with this age within their error margins. In the northern band and intermediate zones, sulfide deposits associated with volcaniclastic rocks predominate, and the limited available data [102,195] indicate an age near the Tournaisian–Visean boundary. An exceptional case is found in the Aljustrel district, where published results [196] suggest some diachrony among the different masses, with a fertile period between ~353 and ~359 Ma. This diachrony and the absence of age data of many ore deposits open up the possibility that the metallogenic activity in the IPB extended over approximately 8 Ma, from the Devonian–Carboniferous boundary to the end of the Tournaisian.

6.9. Nature and Origin of Hydrothermal Fluids

Fluid inclusion studies conducted to date [41,67,198–204] reveal regional salinity values ranging between 2 and 13 wt % NaCl equivalent. These measurements have primarily been taken from quartz in stockwork veins. The values conceal significant variability among different deposits, indicating that a homogeneous mineralizing fluid cannot be considered in the IPB. Although salinity varies, the ranges are more similar to the SEDEX-type deposits than to typical VMS deposits [42,184].

The interpretation of these results suggests several possibilities, including seawater modified by interaction with rocks of the underlying volcano–sedimentary pile [198,199,201,202], basin fluids equilibrated with volcanic and sedimentary rocks over long periods, or magmatic-origin fluids with high salinity and metal content [205], at least for the Sn-Cu mineralization of Neves-Corvo [94,206].

Published $\delta^{18}O$ and δD isotopic data suggest that the hydrothermal fluids responsible for massive sulfide mineralization derive from seawater highly modified by interactions

with underlying magmatic and/or sedimentary rocks [42,129,154,203,206–208]. The resulting fluids would have characteristics similar to connate or basin fluids [42,129]. Tornos and Heinrich [209], and previously Sáez et al. [42], postulated that the sedimentary pile of shales and quartzarenites of the PQ Group represented the main source of hydrothermal fluids. Other authors have suggested significant involvement of magmatic fluids [204,206] or deep metamorphic fluids related to tin-bearing granites, at least for the Sn-Cu mineralization of Neves-Corvo [94,206,210].

6.9.1. Sulfur Source

Available $\delta^{34}S$ data show a wide range of values (–34.2‰ to 12.4‰) for massive sulfides and a narrower range (–4.5‰ to 11.7‰) for stockwork-type mineralizations [151]. Isotopic signatures of massive sulfides with such broad value ranges are more common in SEDEX deposits than in VMS deposits. The analysis of the relationships between S isotopic composition and the textures of massive sulfides reveals an evolution toward heavier signatures parallel to textural evolution [151]. Primitive textures (framboidal and colloform) exhibit lighter S isotopic signatures, whereas sulfides showing more mature textural patterns (idiomorphic crystals, recrystallizations, etc.) have heavier S.

Most authors addressing this topic propose the existence of two sources of reduced S: one generated in situ within the depositional basin by bacterial sulfate reduction (BSR) processes and another of deeper origin carried by hydrothermal fluids [42,43,67,129,136,151,211–213]. This hydrothermal S may also be derived from marine sulfates but the reduction mechanism would be related to inorganic interaction processes at high temperatures with underlying rocks. Although less commonly suggested, a magmatic S source, or at least S equilibrated with magmatic rocks, has also been proposed to explain $\delta^{34}S$ values close to 0‰, which predominate in the higher temperature parageneses of the stockworks [42,151,214].

6.9.2. Metal Source

Pb isotopic composition of IPB massive sulfides indicates a very homogeneous metal source [215]. Regional values exhibit a standard deviation similar to that observed in the Riotinto district [216]. Such a homogeneous lead source could be related to the underlying VSC [217] or to the PQ Group, with minor contribution from the VSC [42]. Tornos and Heinrich [209] reached a similar conclusion based on the modeling of hydrothermal fluids through thermodynamic calculations.

Studies on the provenance of metals using the Re-Os system reveal a clearly defined crustal source in the massive sulfides from Tharsis and Riotinto [190], as well as in Lagoa Salgada, Aljustrel, and Neves-Corvo [191]. However, the initial $^{187}Os/^{188}Os$ ratios around 0.14 in the high-temperature parageneses of the Tharsis and Aznalcóllar stockworks suggest the involvement of a mantle source [189,217], at least for the checked deposits. This could be influenced by the interaction of hydrothermal fluids with mafic magmatic rocks emplaced in epizonal crustal levels.

Isotopic studies based on unconventional isotopes (i.e., Cu, Zn, Fe, and Mo) could provide new insights into the origin of metals in the IPB VMS deposits. Published data are scarce and generally pertain to low-temperature processes with environmental implications [218,219]. The results from the study of samples from Neves-Corvo [220] are inconclusive in this regard. Concerning Mo isotopes, they have been used to discriminate the environmental conditions of two paleogeographically related settings, Filón Norte (Tharsis) and Pozo San Jorge [221].

6.9.3. Hydrothermal Systems

The high concentration of massive sulfide deposits in the IPB requires highly efficient hydrothermal systems from a metallogenetic perspective. Conventional models based on simple convective systems [134,154,222] do not seem capable of generating the enormous deposits found in the IPB [129]. The involvement of basin fluids, primarily stored in

the sediments of the PQ Group and integrated into the hydrothermal circuits, has been proposed as an alternative model [4,42,86,129,209].

The heat required to activate the hydrothermal systems could be related to the dyke and sill system associated with the ascent of a magmatic fluid source of the VSC volcanic rocks [86], an anomalous geothermal gradient associated with the ascent and emplacement of mafic magmas—currently represented by the IPB basalts and dolerites [4,42]—or the plutonic roots of the IPB volcanics [129]. These models, which involve basin fluids stored in thick sedimentary piles, are similar to those proposed for SEDEX-type deposits (e.g., [223]).

There is a widespread consensus regarding the nature of hydrothermal fluids associated with VMS systems. These fluids are chloride-rich, reduced, and moderately acidic solutions [224]. Their specific nature depends on the context in which the system has developed and, consequently, on the nature of the rocks that they are in equilibrium with [224]. The temperature in the deeper zones of the hydrothermal systems has been estimated to range between 300 and 400 °C and decreases dramatically in the near-surface zones of the system [8]. Metals are transported as chloride complexes such as $FeCl^{4-}$ and $FeCl^{2-}$, $CuCl^{2-}$ and $CuCl_3{}^{2-}$, $ZnCl_4{}^{2-}$ and $PbCl^{3-}$, $PbCl_4{}^{2-}$, and $PbCl_2$ [209]. The solubility of metals in this state increases dramatically with temperature, and copper, in particular, has limited potential to enter solutions at temperatures below 350 °C [224]. The potential for co-transport of reduced sulfur and metals in hydrothermal fluids at temperatures below 350 °C is very limited, see [224] and the references therein. Among the common metals in massive sulfides, Fe, Pb, and Zn exhibit high solubility at relatively low temperatures, while Cu requires temperatures >350 °C for efficient transport [224]. Precipitation occurs primarily due to the temperature decreasing and fluid mixing [225].

The application of knowledge derived from studies on both modern and ancient systems on a global scale has been underdeveloped for the specific case of IPB deposits. Tornos and Heinrich [209] propose a model based on solubility and thermodynamic calculations, suggesting that hydrothermal fluids are derived from basinal fluids in equilibrium with the thick detrital sequences characterizing the PQ Group. Although the model is compelling, it was developed with reference to the Filón Norte (Tharsis) deposit, which has some peculiarities that may not be applicable to most IPB deposits.

7. Genetic Model

Metallogenic processes that resulted in the IPB massive sulfide deposits are linked to the regional geodynamic and paleogeographic evolution during the Late Devonian to Mississippian times. The Devonian–Carboniferous transition marked a radical change in the geodynamic context. During the Middle and Upper Devonian, the sediments comprising the PQ Group accumulated in an epicontinental basin dominated by wave and storm activity [30]. At the end of the Devonian, there was a radical shift in the tectonic regime, leading to a compartmentalized basin model with smaller sub-basins undergoing different subsidence rates [33]. The currently most accepted model relates this change to a transtensive regime that resulted in the generation of pull-apart basins, see [15] and the included references. Regardless of the geodynamic regime, the evident regional-scale shift in the geological context during the Devonian–Carboniferous transition was critical for the genesis of the massive sulfide deposits.

From a stratigraphic perspective, sedimentation in a shallow, essentially homogeneous marine basin rapidly changed to black shales and felsic volcaniclastic rocks. The generation and preservation of the sulfide deposits were conditioned by the existence of oxygen-deficient environments and low sedimentation rates. S isotopic data, with the lighter signatures associated with the most primary textures, indicate that BSR processes played an important role in the accumulation of reduced S in depositional environments. Heavier $\delta^{34}S$ values for more evolved textural patterns and the incorporation of metals such as Co and Ni into the hydrothermal fluids suggest a greater involvement of mafic magmatic rocks both in the hydrothermal fluids and the metal contents.

Results from the IBERSEIS seismic profile suggest the emplacement of large volumes of mafic magmas at mid-levels (OMZ) and high levels (SPZ) of the southwestern Iberian crust [44]. In the IPB, the ascent and emplacement of large volumes of mafic magmas created an anomalous geothermal environment that, interacting with a strongly compartmentalized basin [33], favored the development of exceptionally efficient hydrothermal systems. In this general context, and considering the diversity of massive sulfide types known in the IPB, a four-stage metallogenic model is here proposed:

Stage 1: basin compartmentalization and initial sulfide precipitation (Figures 8a,b, 9, and 12a).

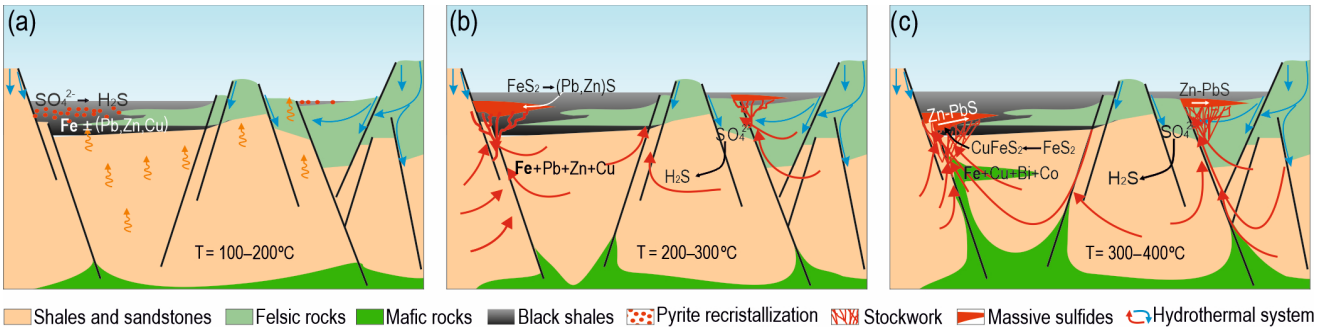

Figure 12. Genetic model based on mineralogical, textural, and geochemical data discussed in the main text. (**a**) Initial development stage of mineralizations dominated by BSR processes in an anomalous geothermal environment at temperatures permitting sulfate-reducing bacteria activity. Oxide and sulfate mineralization occurs on non-oxygen-deficient seafloors. (**b**) Focus of hydrothermal activity through fracture systems and replacement of previously deposited sulfides. In oxidized environments, primary sulfate (barite) and oxide (magnetite and hematite) mineralizations are replaced by sulfides. (**c**) Widespread high-temperature replacement and distillation of mobile phases. During this stage, enrichment in Cu, Au, and Co occurs toward the base of the massive sulfides and the stockwork.

The first stage is related to the compartmentalization of the Late Devonian basin and the generation of oxygen-deficient environments where the activity of BSR induced the initial precipitation of iron sulfides characterized by primary textures (framboidal and colloform). The correlation between these textural types and the highly negative $\delta^{34}S$ values—both in mineralizations associated with black shales and, in some cases, with volcanic rocks—suggests that BSR processes were widespread. Despite this, some sulfide deposits in the northern IPB show evidence of an initial stage in an oxidizing seafloor environment, leading to the precipitation of barite and Fe-oxides, including hematite and magnetite [135]. In this case, the chemocline (redox boundary) is located below the water–sediment interface, and BSR occurs mainly in the interstitial fluids of the underlying rocks or sediments. A similar process, occurring in a very low-temperature hydrothermal environment, has been described by [226] in the Arctic Mid-Oceal Ridge. Here, the first sulfides are produced by hydrothermal replacement of oxidized phases.

The incorporation of high contents of chalcophile elements (Cu, Pb, As, and Sb) into the crystalline lattice of pyrite, as well as their presence in mineral nano-inclusions [127,152], suggests strongly anomalous thermal conditions on the seafloor, as previously suggested by [42,135]. These conditions, while anomalous, were suitable for the survival of sulfate-reducing bacteria (i.e., <100 °C). Although there is no irrefutable evidence, this metallogenic stage could have coincided with regional hydrothermal alteration processes;

Stage 2: recrystallization and hydrothermal activity (Figures 8c,d and 12b).

The second stage involves the recrystallization of sulfides derived from the previous stage within a relatively low-temperature hydrothermal context. During this stage, complete or partial replacement of barite and Fe-oxides generated in more oxidizing environments occurred. The resulting pyrite typically exhibits spongy-looking cores sur-

rounded by a corona limited by crystalline faces. Compositionally, this pyrite appears quite pure, though slightly enriched in Au and Bi [127]. This second stage is associated with the focusing of hydrothermal activity [135] and, consequently, with the initiation of stockwork-type mineralization and the associated hydrothermal alteration;

Stage 3: generalized recrystallization and sulfide replacement (Figures 8e, 9, and 12c).

The third stage represents the widespread recrystallization and partial or total replacement of sulfides from the previous stages. The influence of high-temperature hydrothermal fluids leads to ore-refining processes and the concentration of economically valuable metallic minerals. The resulting parageneses vary significantly from one district to another. Generally, in addition to pyrite, associations of galena, sphalerite, chalcopyrite as interstitial crystals or micro-inclusions in sphalerite (chalcopyrite disease), tetrahedrite–tennantite, arsenopyrite, gold, and electrum are common. Toward the footwall of the massive bodies and in the stockwork zones, this phase often results in significant enrichment in Cu, and in some cases, Co and Au. The pyrite associated with this stage is enriched in Cu, Ag, Ni, Co, As, Zn, Pb, and Sb [127]. This pattern has been observed in deposits associated with black shales (e.g., Tharsis and Masa Valverde) as well as in contexts dominated by volcanic rocks (e.g., Magdalena and Aguas Teñidas). The enrichment of pyrite in mantle-related elements (i.e., Co and Ni), the neoformation of minerals such as cobaltite and gersdorffite, and the initial values of 0.14 for the $^{187}Os/^{188}Os$ ratio measured in parageneses from this stage [189,217] suggest the interaction of hydrothermal fluids with mafic rocks emplaced in epizonal crustal levels;

Stage 4: deformation and metamorphism related to the Variscan Orogeny (Figures 8f, 9 and 10b).

As mentioned earlier, rocks in the IPB underwent intense deformation and low-grade metamorphism during the compressive orogenic phase. The mechanical behavior of sulfides differed significantly under the prevailing pressure and temperature conditions affecting the IPB during this event. Pyrite behaved as a brittle mineral, while other sulfides, including chalcopyrite, galena, sphalerite, and tetrahedrite, behaved ductilely. The consequences for sulfide mineral deposits include the formation of a pseudomylonitic foliation enveloping pyrite crystals, which resemble porphyroclasts with intense brittle fracturing. This texture, common in many studied deposits, can affect both massive sulfides and stockworks, often giving rise to ore shoots heavily enriched in some of these elements. Known examples include the banded copper mineralizations (Rubanée) of Neves-Corvo [94,205], similar lithofacies in Migollas [131,139], or the copper stockwork ("pyroclast") exploited in the Aznalcóllar deposit [41].

8. Conclusions

The following conclusions highlight the progress made in the IPB and the critical areas requiring further investigation to enhance understanding of the geologic history and metallogenic processes.

The general geological framework of the IPB is well understood, with established consensus since the mid-20th century. The IPB's massive sulfides formed in a relatively short period (~8 Ma) between the late Devonian and the Tournaisian–Visean transition. Their deposition was initially controlled by the presence of biologically reduced sulfur linked to BSR processes. This initial depositional phase evolved through subsequent stages of increasing-temperature hydrothermal-fluid injections that provided heavier sulfur and economically significant metals. High-temperature stages facilitated distillation processes and zonal mineral distribution. This mainly contributed to Cu-, Co-, and Au-rich mineralizations in some stockworks and in the base of massive sulfides. At Neves-Corvo, an initial Sn mineralization stage involved different metal and fluid sources compared to other known IPB deposits. A final remobilization stage, related to Variscan compressive phases, played a crucial role in generating high-grade ore shoots in some deposits.

There is a fundamental issue, underlying many other unresolved problems, which deals with the construction of a stratigraphic column useful at a regional scale, with

local variations. Despite recent advances, further correlation between chronostratigraphic and geochronological data is needed to establish the sequence of processes underlying the regional geological context. Correlating the geochronological data with elemental geochemistry of magmatic rocks is also necessary to determine the possible temporal evolution of magmatism in the region.

Generally, a transtensive geodynamic context in a lateral collision environment between the continental masses of Laurussia and Gondwana is accepted. In this setting, pull-apart basins would form, creating environments suitable for the generation and preservation of massive sulfides. Although this proposal seems reasonable, an alternative hypothesis of rifting processes in an extensional context associated with a mantle plume has been underexplored. The temporal evolution of the geochemistry of the mafic rocks implies increasingly deeper mantle sources. This evolution aligns better with a purely extensional context than with a transtensive regime affecting a relatively small area of the Earth's crust.

Regarding magmatism, almost all published studies since the mid-20th century cite bimodal magmatism (felsic–mafic), overlooking the substantial volume of geochemically intermediate (andesitic) rocks in the IPB. The significance of these rocks remains to be studied, as they occur, in part, with the source area of felsic and intermediate rocks. In this regard, the published data suggest a heterogeneous crustal source with very active partial melting processes. If this hypothesis is consistent, the homogeneity in the metal source inferred from Pb isotope geochemistry of sulfide mineralizations needs reevaluation. High-resolution geochemical studies are necessary to advance knowledge in this and other critical areas.

More studies are also required on the nature and physicochemical properties of hydrothermal fluids involved in the genesis of sulfide deposits. Published data indicate relatively low densities for most studied cases. Unless new data alter the current understanding, genetic models based on brine pool systems need revision.

The regional extent of hydrothermal fluid interaction with mantle-derived rocks—as inferred from the Re-Os system for high-temperature mineralizations in the Aznalcóllar and Tharsis districts—is another unresolved aspect. This phenomenon, and similar lesser-studied ones, are critical as they may provide insights into the potential resources of some high-interest technological elements (e.g., Co, Ni, Bi, Sb, In, and Se) scarcely investigated in the IPB.

Author Contributions: Conceptualization: R.S., F.G., T.D., M.T., L.Y., G.R.d.A. and C.M.; Data curation: R.S., F.G., T.D., M.T., L.Y., G.R.d.A. and C.M.; Writing—original draft: R.S. and C.M.; review and editing: F.G., T.D., M.T. and L.Y. All authors have read and agreed to the published version of the manuscript.

Funding: This research received no external funding.

Data Availability Statement: Data are contained within the article.

Acknowledgments: Luís Albardeiro is acknowledged for his kind invitation to participate in the Special Issue "*Mineral Deposits, Geotectonic Evolution and Mineralogical and Geochemical Characterization of Iberian Pyrite Belt—State of the Art*". We are also indebted to the numerous mining companies operating in the Iberian Pyrite Belt for providing us with information, access, and rock samples throughout all our research in the region. The original manuscript was clearly improved thanks to the valuable suggestions and comments of three anonymous reviewers.

Conflicts of Interest: The authors declare no conflicts of interest.

References

1. Leistel, J.M.; Marcoux, E.; Thieblemont, D.; Quesada, C.; Sánchez, A.; Almodóvar, G.R.; Pascual, E.; Sáez, R. The volcanic hosted massive sulphide deposits of the Iberian Pyrite Belt. Review and preface to the special issue. *Miner. Depos.* **1998**, *33*, 2–30. [CrossRef]
2. Pinedo Vara, I. *Piritas de Huelva*; Summa: Madrid, Spain, 1963; p. 1003.
3. IGME. *Síntesis Geológica de la Faja Pirítica del SO de España*; IGME: Madrid, Spain, 1982; p. 106.

4. Sáez, R.; Almodóvar, G.R.; Pascual, E. Geological constraints on massive sulphide genesis in the Iberian Pyrite Belt. *Ore Geol. Rev.* **1996**, *11*, 429–451. [CrossRef]
5. Sáez, R.; Almodóvar, G.R.; Barriga, F.J.A.S. Mineral exploration in the Iberian Pyrite Belt. *SGA News* **1997**, *3*, 7–11.
6. Tornos, F.; Barriga, F.; Marcoux, E.; Pascual, E.; Pons, J.M.; Relvas, J.; Velasco, F. The Iberian Pyrite Belt. In *Data-Base on Global VMS Districts*; Large, R.R., Blundell, D.J., Eds.; CODES-GEODE: Sydney, Australia, 2000; pp. 19–52.
7. Bateman, A.M. Ore deposits of the Rio Tinto (Huelva) district, Spain. *Econ. Geol.* **1927**, *22*, 569–614. [CrossRef]
8. Franklin, J.M.; Gibson, H.L.; Jonasson, I.R.; Galley, A.G. Volcanogenic massive sulfide deposits. In *Encyclopedia of Marine Geosciences*; 100th Anniversary Volume; Springer: Dordrecht, The Netherlands, 2005; pp. 523–560.
9. Rona, P.A.; Scott, S.D. Preface to Special Issue on Sea-Floor Hydrothermal Mineralizations: New Perspectives. *Econ. Geol.* **1993**, *88*, 1935–1976. [CrossRef]
10. Lydon, J.W. Ore deposit models #14, volcanogenic massive sulphide deposits Part 2: Genetic models. *Geosci. Canada* **1988**, *15*, 43–65.
11. Apps, J.A. An Account of the Geology, Petrology and Mineralogy of the San Miguel Concessions and Orebodies in the Province of Huelva, Spain. Ph.D. Thesis, Imperial College, London, UK, 1961; p. 162.
12. Williams, D. Further reflections on the origin of the porphyries and ores of Riotinto, Spain. *Trans. Inst. Min. Metall.* **1962**, *71*, 265–266.
13. Rambaud, F. El sinclinal carbonífero de Rio Tinto (Huelva) y sus mineralizaciones asociadas. *Mem. Inst. Geol. Min. España* **1969**, *71*, 229.
14. Routhier, P.; Aye, F.; Lécolle, M.; Molière, E.P.; Picot, P.; Roger, G. La Ceinture Sud-Ibérique à amas sulfurés dans sa partie espagnole médiane. *Bur. Rech. Géol. Mini. Mem.* **1978**, *94*, 265.
15. Oliveira, J.T.; Quesada, C.; Pereira, Z.; Matos, J.X.; Solá, R.A.; Rosa, D.; Albardeiro, L.; Díez-Montes, A.; Morais, I.; Inverno, C.; et al. South Portuguese Terrane: A continental affinity exotic unit. In *The Geology of Iberia: A Geodynamic Approach*; Quesada, C., Oliveira, J.T., Eds.; Volume 2: The Variscan Cycle; Springer: Berlin/Heidelberg, Germany, 2019; p. 173.
16. Schermerhörn, L.J.G. An outline stratigraphy of the Iberian Pyrite Belt. *Bol. Geol. Min.* **1971**, *82*, 239–268.
17. Delgado, J.F.N. Terrenos paleozoicos de Portugal. Sobre a existencia do terreno siluriano no Baixo Alentejo. *Mem. Acad. Ciênc. Lisboa* **1876**, *1*, 56.
18. Gonzalo Tarín, J. Descripción física, geológica y minera de la provincia de Huelva. In *Memoria de la Comisión del Mapa Geológico de España*; Tercera Parte de la Memoria; Descripción Minera (Classic Reprint): Madrid, Spain, 1878; Volume 2, p. 660.
19. Finlayson, A.M. The pyritic deposits of Huelva, Spain. *Econ. Geol.* **1910**, *5*, 356–372.
20. McGillavry, H.J. The Upper Paleozoic of the Baixo Alemtejo, Southern Portugal. In Proceedings of the 4th Congress on Carboniferous Stratigraphy and Geology, Herlen, The Netherlands, 1958; Volume 2, pp. 395–408.
21. Strauss, G.K. Zur Geologia der Kieslagerstätte Lousal, Portugal. Master's Thesis, University of Munich, Munich, Germany, 1961; p. 87.
22. Strauss, G.K. Sobre la geología de la provincia piritífera del suroeste de la Península Ibérica y de sus yacimientos, en especial sobre la mina de pirita de Lousal (Portugal). *Mem. Inst. Geol. Min. España* **1970**, *77*, 266.
23. van den Boogaard, M. Conodonts of Upper Devonian and Lower Carboniferous from Southern Portugal. *Geol. Mijnb.* **1963**, *42*, 248–259.
24. Colmenero, J.R.; Fernández, L.P.; Moreno, C.; Bahamonde, J.R.; Barba, P.; Heredia, N.; González, F. Carboniferous. In *The Geology of Spain*; Gibbons, W., Moreno, M.T., Eds.; The Geological Society: London, UK, 2002; pp. 93–116.
25. Pruvost, P. Observations sur les terrains dévoniens et carbonifères du Portugal et sur leur faune. *Com. Serv. Geol. Port.* **1912**, *10*, 1–21.
26. van den Boogaard, M.; Schermerhörn, L.J.G. Conodonts faunas from Portugal and southwestern Spain. *Scripta Geol.* **1975**, *28*, 1–41.
27. Oliveira, J.T. The marine Carboniferous of South Portugal. A stratigraphic and sedimentological approach. *Mem. Serv. Geol. Portugal* **1983**, *29*, 3–37.
28. Pereira, Z.; Matos, J.X.; Fernandes, P.; Jorge, R.; Oliveira, J.T. New Lower Givetian age miospores of the Phyllite-Quartzite Group (São Francisco da Serra Anticline IPB Portugal). In Proceedings of the CIMP Faro UALG-LNEG, Faro, Portugal, 2009; pp. 75–78.
29. González, F.; Playford, G.; Moreno, C. Upper Devonian biostratigraphy of the Iberian Pyrite Belt, southwest Spain. Part One: Miospores. *Palaeontographica Abt. B* **2005**, *273*, 1–51. [CrossRef]
30. Sáez, R.; Moreno, C. Geology of the Puebla de Guzmán anticlinorium. In *Geology and VMS Deposits of the Iberian Pyrite Belt*; Barriga, F.J.A.S., Carvalho, D., Eds.; Guidebook Series; Society of Economic Geologists: Littleton, CO, USA, 1997; Volume 27, pp. 131–136.
31. Pereira, Z. Palinoestratigrafia do Sector Sudoeste da Zona Sul Portuguesa. *Comun. Geol.* **1999**, *86*, 25–57.
32. Azor, A.; Dias da Silva, Í.; Gómez Barreiro, J.; González-Clavijo, E.; Martínez Catalán, J.R.; Simancas, J.F.; Martínez Poyatos, D.; Pérez-Cáceres, I.; González Lodeiro, F.; Expósito, I.; et al. *The Geology of Iberia: A Geodynamic Approach*; Quesada, C., Oliveira, J.T., Eds.; Volume 2: The Variscan Cycle; Springer: Berlin/Heidelberg, Germany, 2019; pp. 307–348.
33. Moreno, C.; Sierra, S.; Sáez, R. Evidence for catastrophism at the Famennian–Dinantian boundary in the Iberian Pyrite Belt. In *Recent Advances in Lower Carboniferous Geology*; Strogen, P., Somerville, D., Jones, G.L., Eds.; Geological Society Special Publication: London, UK, 1996; Volume 107, pp. 153–162.

34. Dennison, J.M. Devonian eustatic fluctuations in Euroamerica: Discussions. *Geol. Soc. Am. Bull.* **1985**, *96*, 1595–1597. [CrossRef]
35. Moreno, C.; Sierra, S.; Sáez, R. Mega-debris flows en el tránsito Devónico-Carbonífero de la Faja Pirítica Ibérica. *Geogaceta* **1995**, *17*, 9–11.
36. McGhee, G.R., Jr. *The Late Devonian Mass Extinction: The Frasnian/Famennian Crisis*; Columbia University Press: New York, NY, USA, 1996; 303p.
37. Murphy, A.E.; Sageman, B.B.; Hollander, D.J. Eutrophization by decoupling of the marine biogeochemical cycles of C, N, and P: A mechanism for the Late Devonian mass extinction. *Geology* **2000**, *28*, 427–430. [CrossRef]
38. Kaiser, S.I.; Steuber, T.; Becker, R.T. Environmental change during the Late Famennian and Early Tournaisian (Late Devonian–Early Carboniferous): Implications from stable isotopes and conodont biofacies in southern Europe. *Geol. J.* **2008**, *43*, 241–260. [CrossRef]
39. Moreno, C.; Sáez, R.; González, F. Paleosismicidad asociada al tránsito Devónico–Carbonífero en la Zona Surportuguesa (SW Ibérico). *Geogaceta* **2007**, *43*, 35–38.
40. Sáez, R.; Moreno, C.; González, F.; Toscano, M.; Almodóvar, G.R. *Devonian/Carboniferous Boundary: Tectonic Onset and Massive Sulphide Deposition in the Iberian Pyrite Belt*, 33rd ed.; International Geological Congress: Oslo, Norway, 2008.
41. Almodóvar, G.R.; Sáez, R.; Pons, J.M.; Toscano, M.; Pascual, E. Geology and genesis of the Aznalcóllar massive sulphide deposits, Iberian Pyrite Belt, Spain. *Miner. Depos.* **1998**, *33*, 111–136. [CrossRef]
42. Sáez, R.; Pascual, E.; Toscano, M.; Almodóvar, G.R. The Iberian Type of volcano-sedimentary massive sulphide deposits. *Miner. Depos.* **1999**, *34*, 549–570. [CrossRef]
43. Tornos, F.; Casquet, C.; Relvas, J.M.R.S.; Barriga, F.J.A.S.; Sáez, R. The relationship between ore deposits and oblique tectonics: The SW Iberian Variscan Belt. In *The Timing and Location of Major Ore Deposits in an Evolving Orogen*; Blundell, D.J., Neubauer, F., Von Quadt, A., Eds.; Special Publications, 204; Geological Society: London, UK, 2002; pp. 179–198.
44. Simancas, J.F.; Carbonell, R.; González Lodeiro, F.; Pérez Estaún, A.; Juhlin, C.; Ayarza, P.; Kashubin, A.; Azor, A.; Martínez Poyatos, D.J.; Almodóvar, G.R.; et al. Crustal structure of the transpressional Variscan orogen of SW Iberia: SW Iberia deep seismic reflection profile (IBERSEIS). *Tectonics* **2003**, *22*, 1062. [CrossRef]
45. Simancas, J.F.; Carbonell, R.; González Lodeiro, F.; Pérez Estaún, A.; Juhlin, C.; Ayarza, P.; Kashubin, A.; Azor, A.; Martínez Poyatos, D.J.; Sáez, R.; et al. Transpresional collision tectonics and mantle plume dynamics: The Variscides of southwestern Iberia. In *European Lithosphere Dynamics*; Gee, D.G., Stephenson, R.A., Eds.; Memoirs; Geological Society: London, UK, 2006; Volume 32, pp. 345–354.
46. Giese, U.; Bühn, B. Early Paleozoic rifting and bimodal volcanism in the Ossa Morena Zone of southwest Spain. *Geol. Rundsch.* **1993**, *83*, 143–160. [CrossRef]
47. Lécolle, M. La Ceinture Sud-Ibérique: Un Exemple de Province à Amas Sulfurés Volcano-Sédimentaires (Téctonique, Métamorphisme, Stratigraphie, Volcanisme, Paléogéographie et Métallogénie). Ph.D. Thesis, Université Pierre et Marie Curie, Paris, France, 1977; p. 609.
48. Routhier, P.; Aye, F.; Boyer, C.; Lécolle, M.; Molière, P.; Picot, P.; Roger, G. La ceinture Sud-Iberique à amas sulfurés dans sa partie espagnole médiane. Tableau géologique et métallogénique. Synthèse sur le type amas sulfurés volcano-sédimentaires. *Mem. du BRGM* **1980**, *94*, 265.
49. Oliveira, J.T. The South Portuguese Zone: Stratigraphy and sedimentary tectonism. In *Pre-Mesozoic Geology of Iberia*; Dallmeyer, R.D., Martínez García, E., Eds.; Springer: Berlin/Heidelberg, Germany, 1990; pp. 334–347.
50. Albardeiro, L.; Morais, I.; Matos, J.X.; Solá, R.; Salgueiro, R.; Pereira, Z.; Mendes, M.; Batista, M.J.; de Oliveira, D.; Díez-Montes, A.; et al. Time-Space Evolution of Iberian Pyrite Belt Igneous Activity: Volcanic and Plutonic Lineaments, Geochronology, Ore Horizons and Stratigraphic Constraints. *Gondwana Res.* **2023**, *121*, 235–257. [CrossRef]
51. Moreno, C.; González, F.; Sáez, R.; Sierra, S. Inicio del vulcanismo en el sector de Calañas (Faja Pirítica Ibérica). Datación y caracterización. *Geogaceta* **2003**, *33*, 59–62.
52. Lake, P.A. The Biostratigraphy and Structure of the Pulo Do Lobo Domain and Iberian Pyrite Belt Domain within the Huelva Province. Ph.D. Thesis, University of Southampton, Southampton, UK, 1991; p. 324.
53. Oliveira, J.T.; Pereira, Z.; Carvalho, P.; Pacheco, N.; Korn, D. Stratigraphy of the tectonically imbricated lithological succession of the Neves Corvo mine area, IPB, Portugal. *Miner. Depos.* **2004**, *39*, 422–436. [CrossRef]
54. Oliveira, J.T.; Horn, M.; Paproth, E. Preliminary note on the stratigraphy of the Baixo Alentejo Flysh Group, Carboniferous of Portugal, and on the paleogeographic development compared to corresponding units in northwest Germany. *Com. Serv. Geol. Portugal* **1979**, *65*, 151–168.
55. Simancas, J.F. Coord. La Zona Surportuguesa. In *Geología de España*; Vera, J.A., Ed.; SGE-IGME: Madrid, Spain, 2004; pp. 199–201.
56. Carvalho, D. Consideraçoes sobre o vulcanic¡smo da regiao de Cercal Odemira. Suas relaçoes com a Faixa Piritosa. *Com. Ser. Geol. Portugal* **1976**, *60*, 215–238.
57. Simancas, J.F. Geología de la Extremidad Oriental de la Zona Sudportuguesa. Ph.D. Thesis, University of Granada, Granada, Spain, 1983; p. 439.
58. Rambaud, F. Distribucion de focus volcánicos y yacimientos en la banda pirítica de Huelva. *Bol. Geol. Min.* **1978**, *89*, 223–233.
59. Rosa, D.R.N.; Finch, A.A.; Andersen, T.; Inverno, C.M.C. U–Pb geochronology and Hf isotope ratios of magmatic zircons from the Iberian Pyrite Belt. *Mineral. Petrol.* **2009**, *95*, 47–69. [CrossRef]

60. Pereira, Z. Palinologia E Petrologia Organica Do Sector Sudoeste Da Zona Sul Portuguesa. Ph.D. Thesis, Universidade do Porto, Porto, Portugal, 1997; p. 268.
61. González, F. Las Pizarras Negras Del Límite Devónico/Carbonífero de la Faja Pirítica Ibérica (s.o. De EspañA). Estudio Bioestratigráfico E Implicaciones Sobre la Paleogeografía de la Cuenca Y El Origen de Las Mineralizaciones de Sulfuros. Ph.D. Thesis, Universidad de Huelva, Huelva, Spain, 2004; p. 196.
62. Moreno, C. Postvolcanic Paleozoic of the Iberian Pyrite Belt: An example of basin morphologic control on sediment distribution in a turbidite basin. *J. Sed. Petrol.* **1993**, *63*, 1118–1128. [CrossRef]
63. Moreno, C.; González, F. Estratigrafía de la Zona Sudportuguesa. In *Geología de España*; Vera, J.A., Ed.; SGE-IGME: Madrid, Spain, 2004; pp. 201–205.
64. Mantero, E.M.; García-Navarro, E.; Alonso-Chaves, F.; Martín Parra, L.; Matas, J.; Azor, A. La Zona Sudportuguesa: Propuesta para la división de un bloque continental en dominios. *Geogaceta* **2007**, *43*, 27–30.
65. Aye, F. Géologie ET Gîtes Métallifères de la Moyenne Vallée de L'Odiel (Huelva, Espagne). Ph.D. Thesis, Université Pierre et Marie Curie, Paris, France, 1974; p. 227.
66. Pascual, E.; Sáez, R.; Donaire, T. The Rio Jarama section. In *The Iberian Pyrite Belt. Field Trip Guide*; Tornos, F., Locutura, J., Martins, L., Eds.; Joint SGA IAGOD International Meeting; Field Trip B4; ITGE-IGM: Madrid, Spain, 1999; pp. 39–40.
67. Sánchez-España, J. Mineralogía Y Geoquímica de Yacimientos de Sulfuros Masivos en El áRea Nor-Oriental de la Faja Pirítica Ibérica (San Telmo-San Miguel-Peña del Hierro), Norte de Huelva, España. Ph.D. Thesis, Universidad del País Vasco, Bilbao, Spain, 2000; p. 307.
68. Yusta, I.; Martínez, A.; Velasco, F. Litogeoquímica de las pizarras negras de la Faja Pirítica Ibérica: Implicaciones en la génesis de los sulfuros masivos. *Bol. Soc. Esp. Miner.* **2002**, *25A*, 107–108.
69. Tornos, F.; Solomon, M.; Conde, C.; Spiro, B.F. Formation of the Tharsis massive sulfide deposit, Iberian Pyrite Belt: Geological, lithogeochemical, and stable isotope evidence for deposition in a brine pool. *Econ. Geol.* **2008**, *103*, 185–214. [CrossRef]
70. Sáez, R.; Moreno, C.; González, F.; Almodóvar, G. Black shales and massive sulfides: Causal or casual relationships? Insights from Rammelsberg, Tharsis, and Draa Sfar. *Miner. Depos.* **2011**, *46*, 585–614. [CrossRef]
71. Luz, F.; Mateus, A.; Figueiras, J.; Tassinari, C.C.G.; Ferreira, E.; Gonçalves, L. Recognizing metasedimentary sequences potentially hosting concealed massive sulfide accumulations in the Iberian Pyrite Belt using geochemical fingerprints. *Ore Geol. Rev.* **2019**, *107*, 973–998. [CrossRef]
72. Luz, F.; Mateus, A.; Rosa, C.; Figueiras, J. Geochemistry of Famennian to Visean metapelites from the Iberian Pyrite Belt: Implications for provenance, paleo-redox conditions and vectoring to massive sulfide deposits. *Nat. Resour. Res.* **2020**, *29*, 3613–3652. [CrossRef]
73. Conde, C.; Tornos, F. Geochemistry and Architecture of the Host Sequence of the Massive Sulphides in the Northern Iberian Pyrite Belt. *Ore Geol. Rev.* **2020**, *127*, 103042. [CrossRef]
74. Leistel, J.M.; Marcoux, E.; Deschamps, Y. Chert in the Iberian Pyrite Belt. *Miner. Depos.* **1998**, *33*, 59–81. [CrossRef]
75. Moreno, C.; Sequeiros, L. The Basal Shaly formation of the Iberian Pyrite Belt (South-Portuguese zone): Early carboniferous bituminous deposits. *Palaeogeogr. Palaeoclimatol. Palaeoecol.* **1989**, *73*, 233–241. [CrossRef]
76. Oliveira, J.T.; Wagner-Gentis, C.H.T. The Mértola and Mira formations boundary between Dugueno and Almada de Ouro, Marine Carboniferous of South Portugal. In *Contributions to the Carboniferous Geology and Palaeontology of the Iberian Peninsula*; Lemos de Sousa, J.M., Ed.; University of Porto: Porto, Portugal, 1983; pp. 1–39.
77. Moreno, C.; Sáez, R. Petrología y procedencia de las areniscas del Culm de la parte occidental de la Faja Pirítica Ibérica (Zona Sur-Portuguesa). *Bol. Geol. Min.* **1989**, *100*, 134–147.
78. Moreno, C. Las facies Culm del Anticlinorio de Puebla de Guzmán (Huelva, España). Ph.D. Thesis, Universidad de Granada, Granada, Spain, 1987; p. 375.
79. Munhá, J. Low-grade regional metamorphism in the Iberian Pyrite Belt. *Comun. Serv. Geol. Portugal* **1983**, *69*, 3–35.
80. Mitjavilla, J.; Martí, J.; Soriano, C. Magmatic evolution and tectonic setting of the Iberian Pyrite Belt volcanism. *J. Petrol.* **1997**, *38*, 727–755. [CrossRef]
81. Thiéblemont, D.; Pascual, E.; Stein, G. Magmatism in the Iberian Pyrite Belt: Petrological constraints on a metallogenetic model. *Miner. Depos.* **1997**, *33*, 98–110. [CrossRef]
82. Valenzuela, A.; Donaire, T.; Pin, C.; Toscano, M.; Hamilton, M.A.; Pascual, E. Geochemistry and U-Pb dating of felsic volcanic rocks in the Rio Tinto-Nerva unit, Iberian Pyrite Belt, Spain: Crustal thinning, progressive crustal melting and massive sulphide genesis. *J. Geol. Soc.* **2011**, *168*, 717–732. [CrossRef]
83. IGME. *Mapa Geológico de España*; Escala 1:200.000; Sevilla-Puebla de Guzmán: Madrid, Spain, 2015.
84. McPhie, J.; Doyle, M.; Allen, R.L. *Volcanic Textures: A Guide to the Interpretation of Textures in Volcanic Rocks*; Centre for Ore Deposit and Exploration Studies, University of Tasmania: Hobart, Australia, 1993; 196p.
85. Boulter, C.A. Comparison of Riotinto, Spain, and Guaymas Basin, Gulf of California: An explanation of a supergiant massive sulphide deposit in an ancient sill-sediment complex. *Geology* **1993**, *21*, 801–804. [CrossRef]
86. Boulter, C.A. Extensional tectonics and magmatism as drivers of convection leading to Iberian Pyrite Belt massive sulphide deposits? *J. Geol. Soc.* **1996**, *153*, 181–184. [CrossRef]
87. Soriano, C.; Martí, J. Facies analysis of volcano-sedimentary successions hosting massive sulphide deposits in the Iberian Pyrite Belt, Spain. *Econ. Geol.* **1999**, *94*, 867–882. [CrossRef]

88. Rosa, C.J.P.; McPhie, J.; Relvas, J.M.R.S. Type of volcanoes hosting the massive sulfide deposits of the Iberian Pyrite Belt. *J. Volcanol. Geotherm. Res.* **2010**, *194*, 107–126. [CrossRef]
89. Valenzuela, A.; Donaire, T.; González-Roldán, M.; Toscano, M.; Pascual, E. Volcanic architecture in the Odiel river area and the volcanic environment in the Riotinto-Nerva Unit, Iberian Pyrite Belt, Spain. *J. Volcanol. Geotherm. Res.* **2011**, *202*, 29–46. [CrossRef]
90. Donaire, T.; Pascual, E.; Sáez, R.; Toscano, M. Facies architecture and palaeoenvironmental constraints of subaqueous felsic volcanism in the Iberian Pyrite Belt: The Paymogo Volcano-Sedimentary Alignment. *J. Volcanol. Geotherm. Res.* **2020**, *405*, 107045. [CrossRef]
91. Pascual, E.; Donaire, T.; Toscano, M.; Macías, G.; Pin, C.; Hamilton, M.A. Geochemical and Volcanological Criteria in Assessing the Links between Volcanism and VMS Deposits: A Case on the Iberian Pyrite Belt., Spain. *Minerals* **2021**, *11*, 826. [CrossRef]
92. Rosa, C.J.P.; McPhie, J.; Relvas, J.M.R.S.; Pereira, Z.; Oliveira, T.; Pacheco, N. Facies analysis and volcanic setting of the giant Neves Corvo massive sulfide deposit, Iberian Pyrite Belt, Portugal. *Miner. Depos.* **2008**, *43*, 449–466. [CrossRef]
93. Munhá, J.; Kerrich, R. Sea water-basalt interaction in spilites from the Iberian Pyrite Belt. *Contrib. Mineral. Petrol.* **1980**, *73*, 191–200. [CrossRef]
94. Relvas, J.M.R.S.; Barriga, F.J.A.S.; Ferreira, A.; Noiva, P.C.; Pacheco, N.; Barriga, G. Hydrothermal alteration and mineralization in the Neves-Corvo volcanic-hosted massive sulfide deposit, Portugal. I. Geology, mineralogy, and geochemistry. *Econ. Geol.* **2006**, *101*, 753–790. [CrossRef]
95. Gifkins, C.C.; Herrmann, W.; Large, R.R. *Altered Volcanic Rocks: A Guide to Description and Interpretation*; Centre for Ore Deposit and Exploration Studies, University of Tasmania: Hobart, Australia, 2005; 275p.
96. Díez Montes, A.; Bellido Mulas, F. Magmatismos TTG y Al-K en la Zona Surportuguesa. Relaciones entre plutonismo y vulcanismo. *Geo-Temas* **2008**, *10*, 1449–1452.
97. Amaral, L.J.; Solá, A.R.; Bento Dos Santos, T.M.; Feitoza, L.; Tassinari, C.C.G.; Crispim, L.; Chichorro, M.; Zieger-Hofmann, M.; Gärtner, J.; Linnemann, U.; et al. The bimodal Fii-A2-type and calc-alkaline volcanic sequence of the Aljustrel brownfield region, Iberian Pyrite Belt, SW Iberian Massif. *Geochemistry* **2024**, *84*, 126049. [CrossRef]
98. Soriano, C. Evolució Geodinàmica de la Faja Pirítica Ibérica, Zona Sud Portuguesa. Ph.D. Thesis, Universitat de Barcelona, Barcelona, Spain, 1997; p. 328.
99. Inverno, C.; Ayala, C.; Sousa, P. The Iberian Pyrite Belt: Introduction and geological setting. In *3D, 4D and Predictive Modelling of Major Mineral Belts in Europe*; Weihed, P., Ed.; Springer International Publishing: Cham, Switzerland, 2015; Volume 9, pp. 191–208.
100. Onèzime, J.; Charvet, J.; Faure, M.; Bourdier, J.-L.; Chauvet, A. A new geodynamic interpretation for the South Portuguese Zone (SW Iberia) and the Iberian Pyrite Belt genesis. *Tectonics* **2003**, *22*, 1027. [CrossRef]
101. Albardeiro, L.; Matos, J.X.; Mendes, M.; Solá, R.; Pereira, Z.; Morais, I.; Salgueiro, R.; Pacheco, N.; Araújo, V.; Oliveira, J.T. Geological correlation of Neves-Corvo Mine and Pomarão Antiform sequences (Iberian Pyrite Belt, Portugal). *Comun. Geol.* **2020**, *107*, 111–132.
102. Barrie, C.T.; Amelin, Y.; Pascual, E. U-Pb geochronology of VMS mineralization in the Iberian Pyrite Belt. *Miner. Depos.* **2002**, *37*, 684–703. [CrossRef]
103. Codeço, M.S.; Mateus, A.; Figueiras, J.; Rodrigues, P.; Gonçalves, L. Development of the Ervidel-Roxo and Figueirinha-Albernoa volcanic sequences in the Iberian Pyrite Belt, Portugal: Metallogenic and geodynamic implications. *Ore Geol. Rev.* **2018**, *98*, 80–108. [CrossRef]
104. Donaire, T.; Pascual, E.; Sáez, R.; Pin, C.; Hamilton, M.A.; Toscano, M. Geochemical and Nd isotopic signature of felsic volcanic rocks as a proxy of volcanic-hosted massive sulphide deposits in the Iberian Pyrite Belt (SW, Spain): The Paymogo Volcano-Sedimentary Alignment. *Ore Geol. Rev.* **2020**, *120*, 103408. [CrossRef]
105. Cravinho, A.; Rosa, D.; Relvas, J.M.R.S.; Solá, A.R.; Pereira, I.; Paquette, J.-L.; Borba, M.L.; Tassinari, C.C.G.; Chew, D.; Drakou, F.; et al. From source to surface: Clues from garnet-bearing Carboniferous silicic volcanic rocks, Iberian Pyrite Belt, Portugal. *Contrib. Mineral. Petrol.* **2024**, *179*, 32. [CrossRef]
106. Rosa, D.; Inverno, C.; Oliveira, V.; Rosa, C. Geochemistry of volcanic rocks Albernoa area IPB Portugal. *Inter. Geol. Rev.* **2004**, *46*, 366–383. [CrossRef]
107. Pereira, Z.; Matos, J.X.; Solá, A.R.; Batista, M.J.; Salgueiro, R.; Rosa, C.; Oliveira, J.T. Geology of the recently discovered massive and stockwork sulphide mineralization at Semblana, Rosa Magra and Monte Branco, Neves–Corvo mine region, Iberian Pyrite Belt, Portugal. *Geol. Mag.* **2021**, *158*, 1253–1268. [CrossRef]
108. de Mello, C.R.; Tornos, F.; Conde, C.; Tassinari, C.C.G.; Farci, A.; Vega, R. Geology, Geochemistry, and Geochronology of the Giant Rio Tinto VMS Deposit, Iberian Pyrite Belt, Spain. *Econ. Geol.* **2022**, *117*, 1149–1177. [CrossRef]
109. Sun, S.; McDonough, W.F. Chemical and isotopic systematics of oceanic basalts: Implications for mantle composition processes. *Geol. Soc. Spec. Pub.* **1989**, *42*, 313–345. [CrossRef]
110. Munhá, J. Blue amphiboles, metamorphic regime, and plate tectonic modelling in the Iberian Pyrite Belt. *Contrib. Mineral. Petrol.* **1979**, *69*, 279–289. [CrossRef]
111. Dallmeyer, R.D.; Fonseca, P.; Quesada, C.; Ribeiro, A. $^{40}Ar/^{39}Ar$ mineral age constraints for the tectonothermal evolution of a Variscan suture in southwest Iberia. *Tectonophysics* **1993**, *222*, 177–194. [CrossRef]
112. Crespo, A.; Orozco, M. The Southern Iberia Shear Zone: A major boundary in the Hercynian folded belt. *Tectonophysics* **1988**, *148*, 221–227. [CrossRef]

113. Silva, J.B.; Oliveira, J.T.; Ribeiro, A. Structural outline of the South Portuguese Zone. In *Pre-Mesozoic Geology of Iberia*; Dallmeyer, R.D., Martínez-García, E., Eds.; Springer: Heidelberg, Germany, 1990; pp. 348–362.
114. Quesada, C. A reappraisal on the structure of the Spanish segment of the Iberian Pyrite Belt. *Miner. Depos.* **1998**, *33*, 31–44. [CrossRef]
115. Martin-Izard, A.; Arias, D.; Arias, M.; Gumiel, P.; Sanderson, D.J.; Castañon, C.; Sanchez, J. Ore deposit types and tectonic evolution of the Iberian Pyrite Belt: From transtensional basins and magmatism to transpression and inversion tectonics. *Ore Geol. Rev.* **2016**, *79*, 254–267. [CrossRef]
116. Quesada, C.; Braid, J.A.; Fernandes, P.; Ferreira, P.; Jorge, R.S.; Matos, J.X.; Murphy, J.B.; Oliveira, J.T.; Pedro, J.; Pereira, Z. SW Iberia Variscan suture Zone: Oceanic affinity units. In *The Geology of Iberia: A Geodynamic Approach*; Quesada, C., Oliveira, J.T., Eds.; Volume 2: The Variscan Cycle; Springer: Berlin/Heidelberg, Germany, 2019; pp. 131–172.
117. Paslawski, L.E.; Braid, J.A.; Quesada, C.; McFarlane, C.M. Geochronology of the Iberian Pyrite Belt and the Sierra Norte Batholith: Lower Plate Magmatism during Supercontinent Amalgamation? *J. Geol. Soc. Lond. Spec. Publ.* **2020**, *503*, 589–617. [CrossRef]
118. Quesada, C.; Fonseca, P.; Munhá, J.; Oliveira, J.T.; Ribeiro, A. The Beja—Acebuches Ophiolite (Southern Iberia Variscan fold belt): Geological characterization and geodynamic significance. *Bol. Geol. Min.* **1994**, *105*, 3–49.
119. Möller, P.; Dieterle, M.A.; Dulski, P.; German, K.; Schneider, H.J.; Schultz, W. Geochemical proximity indicators of massive sulphide mineralization in the Iberian Pyrite Belt and the East Pontic Metallotect. *Miner. Depos.* **1983**, *18*, 387–398. [CrossRef]
120. Sáez, R. Geología Y Mineralizaciones de Sn-W de la Región Del Bajo Corumbel (La Palma del Condado, Huelva). Bachelor's Thesis, Universidad de Sevilla, Sevilla, Spain, 1986; p. 210.
121. Sáez, R.; Almodóvar, G.R.; Pascual, E. Mineralizaciones estratoligadas de scheelita en la Faja Pirítica del SO Ibérico. *Bol. Soc. Esp. Miner.* **1988**, *11*, 135–141.
122. Sáez, R.; Requena, A.; Fernández-Caliani, J.C.; Almodóvar, G.R. Control estructural de las mineralizaciones de Sn-W-As del Bajo Corumbel, La Palma del Condado, Huelva. *Stud. Geol. Sal.* **1989**, *4*, 189–203.
123. Sáez, R.; Alonso-Chaves, F. Control estructural de las mineralizaciones del grupo La Ratera-Masegoso. *Bol. Soc. Esp. Miner.* **1998**, *21*, 186–187.
124. German, K.; Lüders, V.; Banks, D.A.; Simon, K.; Hoefs, J. Late Hercynian polymetallic mineralization in the Iberian Pyrite Belt: Fluid inclusion and stable isotope geochemistry (S-O-H-Cl). *Miner. Depos.* **2003**, *38*, 953–967. [CrossRef]
125. Blanco, A.; Rothenberg, B. *Exploración Arqueometalúrgica de Huelva*; Labor: Barcelona, Spain, 1981; p. 312.
126. Sáez, R.; Nocete, F.; Nieto, J.M.; Capitán, M.A.; Rovira, S. The extractive metallurgy of copper from Cabezo Juré, Huelva, Spain: Chemical and mineralogical study of slags dated to the Third Millennium B.C. *Can. Mineral.* **2003**, *41*, 627–638. [CrossRef]
127. Yesares, L.; Piña, R.; González-Jiménez, J.M.; Sáez, R.; Ruíz de Almodóvar, G.; Fanlo, I.; Manuel Pons, J.; Vega, R. Distribution of critical metals in evolving pyrite from massive sulfide ores of the Iberian Pyrite Belt. *Ore Geol. Rev.* **2023**, *153*, 105275. [CrossRef]
128. Carvalho, J.R.S.; Relvas, J.M.R.S.; Pinto, A.M.M.; Frenzel, M.; Krause, J.; Gutzmer, J.; Pacheco, N.; Fonseca, R.; Santos, S.; Caetano, P.; et al. Indium and selenium distribution in the Neves-Corvo deposit, Iberian Pyrite Belt, Portugal. *Mineral. Mag.* **2018**, *82*, 5–41. [CrossRef]
129. Tornos, F. Environment of formation and styles of volcanogenic massive sulfides: The Iberian Pyrite Belt. *Ore Geol. Rev.* **2006**, *28*, 259–307. [CrossRef]
130. Relvas, J.M.R.S.; Barriga, F.J.A.S.; Pinto, A.; Ferreira, A.; Pacheco, A.; Noiva, P.C.; Barriga, G.; Baptista, R.; Carvalho, D.; Oliveira, V.; et al. The Neves Corvo deposit, Iberian Pyrite Belt, Portugal: Impacts and future, 25 years after discovery. *Soc. Econ. Geol. Spec. Publ.* **2002**, *9*, 155–176.
131. Santos, A.; Caballero, B.; Prada, J.M. Descripción geológica de los yacimientos de Sotiel Coronada. *Bol. Geol. Min.* **1996**, *107*, 31–38.
132. Strauss, G.K.; Roger, G.; Lécolle, M.; Lopera, E. Geochemical and geologic study of the volcano-sedimentary sulfide orebody of La Zarza, Huelva province, Spain. *Econ. Geol.* **1981**, *76*, 1975–2000. [CrossRef]
133. Barriga, F.J.A.S. Hydrothermal Metamorphism and Ore Genesis at Aljustrel, Portugal. Ph.D. Thesis, University Western Ontario, London, ON, Canada, 1983; p. 386.
134. Barriga, F.J.A.S.; Fyfe, W.S. Giant pyritic base-metal deposits: The example of Feitais (Aljustrel, Portugal). *Chem. Geol.* **1988**, *69*, 331–343. [CrossRef]
135. Almodóvar, G.; Yesares, L.; Sáez, R.; Toscano, M.; González, F.; Pons, J.M. Massive sulfide ores in the Iberian pyrite belt: Mineralogical and textural evolution. *Minerals* **2019**, *9*, 653. [CrossRef]
136. Tornos, F.; González Clavijo, E.; Spiro, B. The Filón Norte orebody, Tharsis, Iberian Pyrite Belt: A proximal low-temperature shale hosted massive sulphide in a thin-skinned tectonic belt. *Miner. Depos.* **1998**, *33*, 150–169. [CrossRef]
137. González, F.; Moreno, C.; Sáez, R.; Clayton, G. Ore genesis age of the Tharsis Mining District (Iberian Pyrite Belt): A palynological approach. *J. Geol. Soc.* **2002**, *159*, 229–232. [CrossRef]
138. Ferreira da Silva, E.; Bobos, I.; Matos, J.X.; Patinha, C.; Reis, A.P.; Cardoso, E. Mineralogy and geochemistry of trace metals and REE in volcanic massive sulfide host rocks, stream sediments, stream waters and acid mine drainage from the Lousal mine area (Iberian Pyrite Belt, Portugal). *Appl. Geochem.* **2009**, *24*, 383–401. [CrossRef]
139. González, F.; Moreno, C.; Santos, A. The massive sulphide event in the Iberian Pyrite Belt: Confirmatory evidence from the Sotiel-Coronada. *Mine. Geol. Mag.* **2006**, *143*, 821–827. [CrossRef]

140. Ruiz, C.; Arribas, A.; Arribas, A., Jr. Mineralogy and geochemistry of the Masa Valverde blind massive sulphide deposit, Iberian Pyrite Belt (Spain). *Ore Geol. Rev.* **2002**, *19*, 1–22. [CrossRef]
141. Sáez, R.; Moreno, C.; González, F. Synchronous deposition of massive sulphide deposits in the Iberian Pyrite Belt: New data from Las Herrerías and La Torerera ore-bodies. *C. R. Geosci.* **2008**, *340*, 829–839. [CrossRef]
142. García Palomero, F. *Caracteres Geológicos y Relaciones Morfológicas y Genéticas de Las Mineralizaciones Del Anticlinal de Riotinto*; Excma Diputación; Instituto Estudios Onubenses "Padre Marchena": Huelva, Spain, 1980; p. 264.
143. Knight, F.C. The Mineralogy, Geochemistry and Genesis of Secondary Sulphide Mineralization of the Las Cruces, Spain. Ph.D. Thesis, University Wales, Cardiff, UK, 2000; p. 434.
144. García de Miguel, J.M. Mineralogía, paragénesis y sucesión de los sulfuros masivos de la Faja Pirítica en el suroeste de la Península Ibérica. *Bol. Geol. Min.* **1990**, *101*, 73–105.
145. Marcoux, E.; Moelo, Y. Comparative mineralogy of massive and stringer sulphide ore deposits in Southern Spain. In *Current Research in Geology Applied to Ore Deposits*; Fenoll Hach-Ali, P., Torres Ruiz, J., Gervilla, F., Eds.; University Granada: Granada, Spain, 1993; pp. 343–345.
146. Marcoux, E.; Moelo, Y.; Leistel, J.M. Bismuth and cobalt minerals: Indicators of stringer zones to massive-sulfide deposits, South Iberian Pyrite Belt. *Miner. Depos.* **1996**, *31*, 1–26. [CrossRef]
147. Gaspar, O.C. Mineralogy and sulfide mineral chemistry of the Neves-Corvo ores, Portugal: Insight into their genesis. *Can. Mineral.* **2002**, *40*, 611–636. [CrossRef]
148. Fernández Álvarez, G. Los Yacimientos de Sulfuros Polimetálicos Del s.o. Ibérico Y Sus Métodos de Prospección. Ph.D. Thesis, University of Salamanca, Salamanca, Spain, 1974; p. 844.
149. Barrett, T.J.; Dawson, G.L.; MacLean, W.H. Volcanic stratigraphy, alteration, and sea-floor setting of the Paleozoic Feitais massive sulfide deposit, Aljustrel, Portugal. *Econ. Geol.* **2008**, *103*, 215–239. [CrossRef]
150. García de Miguel, J.M.; Chamorro, R. Geología y mineralogía del yacimiento de Sierrecilla (Puebla de Guzmán, Huelva, España). *Bol. Geol. Min.* **1986**, *97*, 510–520.
151. Velasco, F.; Sánchez-España, J.; Boyce, A.J.; Fallick, A.E.; Sáez, R.; Almodóvar, G.R. A new sulphur isotopic study of some IPB deposits: Evidence of a textural control on sulphur isotope composition. *Miner. Depos.* **1998**, *34*, 14–18. [CrossRef]
152. González-Jiménez, J.M.; Yesares, L.; Piña, R.; Sáez, R.; Almodóvar, G.R.; Nieto, F.; Tenorio, S. Polymetallic nanoparticles in pyrite from VMS deposits of the Iberian Pyrite Belt. *Ore Geol. Rev.* **2022**, *145*, 104875. [CrossRef]
153. Barriga, F.J.A.S.; Carvalho, D. Carboniferous volcanogenic sulfide mineralization in south Portugal, Iberian pyrite belt. *Com. Serv. Geol. Port.* **1983**, *29*, 99–113.
154. Munhá, J.; Barriga, F.J.A.S.; Kerrich, R. High ^{18}O ore-forming fluids in volcanic hosted base metal massive sulphide deposits: Geologic, $^{18}O/^{16}O$, and D/H evidence for the Iberian Pyrite Belt; Crandon, Wisconsin; and Blue Hill, Maine. *Econ. Geol.* **1986**, *81*, 530–552. [CrossRef]
155. Jorge, R.S. Caracterização Petrográfica, Geoquímica E Isotópica Dos Reservatórios Metalíferos Crustais, Dos Processos de Extracção de Metais E Dos Fluidos Hidrotermais Envolvidos Em Sistemas Mineralizantes Híbridos NA Faixa Piritosa Ibérica. Ph.D. Thesis, Universidade de Lisboa, Lisboa, Portugal, 2010; p. 324.
156. Plimer, I.R.; Carvalho, D. The geochemistry of hydrothermal alteration at the Salgadinho copper deposit, Portugal. *Miner. Depos.* **1982**, *17*, 193–211. [CrossRef]
157. Toscano, M.; Almodóvar, G.R.; Pascual, E.; Sáez, R. Hydrothermal alteration related to the "Masa Valverde" massive sulphide deposit, Iberian Pyrite Belt, Spain. In *Current Research in Geology Applied to Ore Deposits*; Fenoll Hach-Ali, P., Torres Ruiz, J., Gervilla, F., Eds.; University Granada: Granada, Spain, 1993; pp. 389–392.
158. Toscano, M.; Almodóvar, G.R.; Sáez, R.; Nieto, J.M.; Escobar, J.M. Mineralogy and geochemistry of hydrothermal alteration in the stockwork of Atalaya (Rio Tinto, Huelva). *Bol. Soc. Esp. Min.* **2002**, *23*, 212–215.
159. Almodóvar, G.R.; Sáez, R.; Toscano, M.; Pascual, E. Co-Ni and "inmobile" element behaviour in ancient hydrothermal systems, Aznalcóllar, Iberian Pyrite Belt, Spain. In *Mineral Deposits: From Their Origin to Their Environmental Impacts*; Pašava, J., Kríbek, R., Zák, K., Eds.; Balkema: Rotterdam, The Netherlands, 1995; pp. 217–220.
160. Sánchez-España, J.; Velasco, F.; Yusta, I. Hydrothermal alteration of felsic volcanic rocks associated with massive sulphide deposition in the northern Iberian Pyrite Belt (SW Spain). *Appl. Geochem.* **2000**, *15*, 1265–1290. [CrossRef]
161. Toscano, M. Alteración Hidrotermal Asociada a Los Yacimientos de Sulfuros Masivos de la Faja Pirítica Suribérica. Ph.D. Thesis, Universidad de Huelva, Huelva, Spain, 2015; p. 224.
162. Almodóvar, G.R.; Sáez, R. Los sulfuros masivos de la Faja Pirítica Ibérica. In *Geología de España*; Vera, J.A., Ed.; SGE-IGME: Madrid, Spain, 2004; pp. 207–209.
163. Barriga, F.J.A.S.; Relvas, J.M.R.S. Hydrothermal alteration an exploration criterion in the IPB: Facts, problems and future. In *Symposium Polymetallic Sulphides of the Iberian Pyrite Belt*; Universidade de Evora: Evora, Portugal, 1993; pp. 1.3.1–1.3.2.
164. Inverno, C.M.; Solomon, M.; Barton, M.D.; Foden, J. The Cu stockwork and massive sulfide ore of the Feitais volcanic-hosted massive sulfide deposit, Aljustrel, Iberian Pyrite Belt, Portugal: A mineralogical, fluid inclusion, and isotopic investigation. *Econ. Geol.* **2008**, *103*, 241–267. [CrossRef]
165. Toscano, M.; Sáez, R.; Almodóvar, G.R. Carbonatos hidrotermales asociados al depósito de sulfuros masivos "Masa Valverde" (Faja Pirítica Ibérica): Características texturales y geoquímicos. *Cuad. Lab. Xeol. Laxe* **2000**, *25*, 211–214.

166. Locutura, J. The La Zarza mine. In *The Iberian Pyrite Belt*; Tornos, F., Locutura, J., Martins, L., Eds.; Joint SGA-IAGOD International Meeting 1999; Field Trip B4; ITGE-IGM: Madrid, Spain, 1999; p. 49.
167. Nesbitt, R.W.; Pascual, E.; Fanning, C.M.; Toscano, M.; Sáez, R.; Almodóvar, G.R. U-Pb dating of stockwork zircons from the eastern Iberian Pyrite Belt. *J. Geol. Soc.* **1999**, *156*, 7–10. [CrossRef]
168. Toscano, M.; Pascual, E.; Nesbitt, R.W.; Almodóvar, G.R.; Sáez, R.; Donaire, T. Geochemical discrimination of hydrothermal and igneous zircon in the Iberian Pyrite Belt, Spain. *Ore Geol. Rev.* **2014**, *56*, 301–311. [CrossRef]
169. Williams, P.A. *Oxide Zone Geochemistry*; Ellis Harwood: New York, NY, USA, 1990; 286p.
170. Boyle, D.R. Preglacial Weathering of Massive Sulfide Deposits in the Bathurst Mining Camp: Economic Geology, Geochemistry, and Exploration Applications. In *Massive Sulphide Deposits of the Bathurst Mining Camp, New Brunswick, and Northern Maine*; Goodfellow, W.D., McCutcheon, S.R., Peter, J.M., Eds.; Economic Geology Monograph; Society of Economic Geologists: Littleton, CO, USA, 2003; Volume 11, pp. 689–721.
171. Arribas, A. Los Yacimientos de Oro Asociados con las Monteras Limoníticas de la FPI. *Bol. Geol. Min.* **1998**, *109*, 429–434.
172. Yesares, L.; Sáez, R.; Nieto, J.M.; Almodóvar, G.R.; Gómez, C.; Escobar, J.M. The Las Cruces Deposit, Iberian Pyrite Belt, Spain. *Ore Geol. Rev.* **2015**, *66*, 25–46. [CrossRef]
173. Capitán, M.A. Mineralogía y Geoquímica de la Alteración Superficial de Depósitos de Sulfuros Masivos en la Faja Pirítica Ibérica. Ph.D. Thesis, Universidad de Huelva, Huelva, Spain, 2006; 260p.
174. Velasco, F.; Herrero, J.M.; Suárez, S.; Yusta, I.; Álvaro, A.; Tornos, F. Supergene Features and Evolution of Gossans Capping Massive Sulphide Deposits in the Iberian Pyrite Belt. *Ore Geol. Rev.* **2013**, *53*, 181–203. [CrossRef]
175. Andrew, R.L. *Short Course in Evaluation of Gossans in Mineral Exploration*; ADIMB: Brasilia, Brazil, 2000; 57p.
176. Oliveira, V.; Matos, J.; Bengala, M.; Silva, N.; Sousa, P.; Torres, L. Geology and Geophysics as Successful Tools in the Discovery of the Lagoa-Salgada Orebody (Sado Tertiary Basin-Iberian Pyrite Belt), Grandola, Portugal. *Miner. Depos.* **1998**, *33*, 170–189. [CrossRef]
177. Kinkel, A.R., Jr. Observations on the pyrite deposits of the Huelva district, Spain, and their relationships to volcanism. *Econ. Geol.* **1962**, *57*, 1071–1080. [CrossRef]
178. Carvalho, D. Geologia, metalogenia e metodologia da investigaçao de sulfuretos polimetálicos do Sul do Portugal. Comun. *Serv. Geol. Port.* **1979**, *65*, 169–191.
179. Barriga, F.J.A.S. Metallogenesis in the Iberian Pyrite Belt. In *Pre-Mesozoic Geology of Iberia*; Dallmeyer, R.D., Martínez-García, E., Eds.; Springer: Berlin, Germany, 1990; pp. 369–379.
180. Sato, T. Behaviours of ore-forming solutions in seawater. *Mining Geol.* **1972**, *22*, 31–42.
181. Solomon, M. 'Volcanic' massive sulphide deposits and their host rocks—A review and an explanation. In *Handbook of Strata-Bound and Stratiform Ore Deposits, II, Regional Studies and Specific Deposits*; Wolf, K.A., Ed.; Elsevier: Amsterdam, The Netherlands, 1976; pp. 21–50.
182. Francheteau, J.; Needham, H.D.; Choukroune, P.; Juteau, T.; Seguret, M.; Ballard, R.D.; Fox, J.P.; Normark, W.; Carranza, A.; Cordoba, D.; et al. Massive deep-sea sulphide ore deposits discovered on the East Pacific Rise. *Nature* **1979**, *277*, 523–528. [CrossRef]
183. Finlow-Bates, T. The chemical and physical controls on the genesis of submarine exhalative orebodies and their implications for formulating exploration concepts: A review. *Geol. Jahrb.* **1980**, *40*, 131–168.
184. Franklin, J.M.; Sangster, D.F.; Lydon, J.W. Volcanogenic massive sulfide deposits. In *Economic Geology*; 75th Anniversary Volume; SEG: Littleton, CO, USA, 1981; pp. 485–627.
185. Urabe, T. Kuroko deposit modelling based on magmatic hydrothermal theory. *Mining Geol.* **1987**, *37*, 159–176.
186. Large, R.R. Australian volcanic-hosted massive sulfide deposits: Features, styles, and genetic models. *Econ. Geol.* **1992**, *87*, 471–510. [CrossRef]
187. Barrie, C.T.; Hannington, M.D. Classification of volcanic-associated massive sulfide deposits based on host-rock composition. In *Volcanic-Associated Massive Sulphide Deposits: Processes and Examples in Modern and Ancient Settings*; Barrie, C.T., Hanningtonm, N.D., Eds.; Reviews in Economic Geology; SEG: Littleton, CO, USA, 1999; Volume 8, pp. 1–11.
188. Stein, H.J.; Morgan, J.W.; Scherstén, A. Re-Os dating of low-level highly-radiogenic (LLHR) sulfides: The Harnas gold deposit, southwest Sweden records continental scale tectonic events. *Econ. Geol.* **2000**, *95*, 1657–1671. [CrossRef]
189. Nieto, J.M.; Almodóvar, G.R.; Pascual, E.; Sáez, R.; Jagoutz, E. Evidencias isotópicas sobre el origen de los metales en los sulfuros masivos de la Faja Pirítica Ibérica. *Cuad. Lab. Xeol. Laxe* **2000**, *25*, 139–142.
190. Mathur, R.; Ruiz, J.; Tornos, F. Age and sources of the ore at Tharsis and Rio Tinto, Iberian Pyrite Belt, from Re-Os isotopes. *Miner. Depos.* **1999**, *34*, 790–793. [CrossRef]
191. Munhá, J.; Relvas, J.M.R.S.; Barriga, F.J.A.S.; Conceição, P.; Jorge, R.C.G.S.; Mathur, R.; Ruiz, J.; Tassinari, C.C.G. Os isotope systematics in the Iberian Pyrite Belt. In *Mineral Deposit Research: Meeting the Global Challenge*; Mao, J., Bierlein, F.P., Eds.; Springer: Berlin, Germany, 2005; Volume 1, pp. 663–666.
192. Pereira, Z.; Sáez, R.; Pons, J.M.; Oliveira, J.T.; Moreno, C. Edad devónica (Struniense) de las mineralizaciones de Aznalcóllar (Faja Pirítica Ibérica) en base a palinología. *Geogaceta* **1996**, *20*, 1609–1612.
193. Li, X.; Zhao, K.D.; Jiang, S.Y.; Palmer, M.R. In-situ U-Pb Geochronology and Sulfur Isotopes Constrain the Metallogenesis of the Giant Neves Corvo Deposit, Iberian Pyrite Belt. *Ore Geol. Rev.* **2019**, *105*, 223–235. [CrossRef]

194. Pereira, Z.; Pacheco, N.; Oliveira, J. A case of applied palynology: Dating the lithological succession of the Neves Corvo Mine, Iberian Pyrite Belt, Portugal. In Proceedings of the XVth International Congress on Carboniferous and Permian Stratigraphy, Utrecht, The Netherlands, 2003; Abstracts Book, pp. 397–401.
195. Dunning, G.R.; Díez Montes, A.; Matas, J.; Martín Parra, L.M.; Almarza, J.; Donaire, M. Geocronología U/Pb del vulcanismo ácido y granitoides de la Faja Pirítica Ibérica (Zona Surportuguesa). *Geogaceta* **2002**, *32*, 127–130.
196. Amaral, L.J.; Solá, A.R.; Bento dos Santos, T.M.; Tassinari, C.C.G.; Gonçalves, J. U-Pb zircon SHRIMP dating of a protracted magmatic setting and its volcanic emplacement: Insights from the felsic volcanic rocks hosting the sulphide ore of the giant Aljustrel Deposit, Iberian Pyrite Belt. *Ore Geol. Rev.* **2021**, *134*, 104147. [CrossRef]
197. Streel, M.; Higgs, K.; Loboziak, S.; Riegel, W.; Steemans, P.H. Spore Stratigraphy and Correlation with Faunas and Floras in the Type Marine Devonian of the Ardenne-Rhenish Regions. *Rev. Palaeobot. Palynol.* **1987**, *50*, 211–229. [CrossRef]
198. Bobrowicz, G.L. Mineralogy, Geochemistry and Alteration as Exploration Guides at Aguas Teñidas Este, Pyrite Belt, Spain. Ph.D. Thesis, University of Birmingham, Birmingham, UK, 1995; p. 424.
199. Toscano, M.; Sáez, R.; Almodóvar, G.R. Evolución de los fluidos hidrotermales en la génesis de los sulfuros masivos de Aznalcóllar (Faja Pirítica Ibérica): Evidencias a partir de inclusiones fluidas. *Geogaceta* **1997**, *21*, 211–214.
200. Moura, A.; Noronha, F.; Cathelineau, M.; Boiron, M.C.; Ferreira, A. Evidence of metamorphic fluid migration within the Neves Corvo ore deposits: The fluid inclusion data. In Proceedings of the SEG Neves Corvo Field Conference, Lisbon, Portugal, 11–14 May 1997; pp. 11–14.
201. Nehlig, P.; Cassard, D.; Marcoux, E. Geometry and genesis of feeder zones of massive sulphide deposits: Constraints from the Río Tinto ore deposits (Spain). *Miner. Depos.* **1998**, *33*, 137–149. [CrossRef]
202. Inverno, C.; Lopes, C.; D'Orey, F.; Carvalho, D. The Cu (Au) stockwork deposit of Salgadinho, Cercal, Portugal, Pyrite Belt, SW Portugal—Paragenetic sequence and fluid inclusion investigation. In *Volcanic Environments and Massive Sulfide Deposits, Program and Abstracts*; Gemmell, J.B., Pongratz, J., Eds.; CODES, Special Publication: Sydney, Australia, 2000; pp. 99–101.
203. Sánchez-España, J.; Velasco, F.; Boyce, A.J.; Fallick, A.E. Source and evolution of ore-forming hydrothermal fluids in the northern Iberian Pyrite Belt massive sulphide deposits (SW Spain): Evidence from fluid inclusions and stable isotopes. *Miner. Depos.* **2003**, *38*, 519–537. [CrossRef]
204. Moura, A. Fluids from the Neves Corvo massive sulphide ores, Iberian Pyrite Belt, Portugal. *Chem. Geol.* **2005**, *223*, 153–169. [CrossRef]
205. Solomon, M.; Quesada, C. Zn-Pb-Cu massive sulfide deposits: Brine pool types occur in collisional orogens, black smoker types occur in backarc/arc basins. *Geology* **2003**, *31*, 1029–1032. [CrossRef]
206. Relvas, J.M.R.S.; Tassinari, C.C.G.; Munhà, J.; Barriga, F.J.A.S. Multiple sources for ore-forming fluids in the Neves Corvo VHMS deposit of the Iberian Pyrite Belt (Portugal): Strontium, neodymium and lead isotope evidence. *Miner. Depos.* **2001**, *36*, 416–427. [CrossRef]
207. Barriga, F.J.A.S.; Kerrich, R. Extreme 18O-enriched volcanics and 18O-evolved marine water, Aljustrel, Iberian Pyrite Belt: Transition from high to low Rayleigh number convective regimes. *Geochim. Cosmochim. Acta* **1984**, *48*, 1021–1031. [CrossRef]
208. Fouillac, A.M.; Javoy, M. Oxygen and hydrogen isotopes in the volcano-sedimentary complex of Huelva (Iberian Pyrite Belt): Example of water circulation through a volcano-sedimentary sequence. *Earth Planet. Sci. Lett.* **1988**, *87*, 473–484. [CrossRef]
209. Tornos, F.; Heinrich, C.A. Shale basins, sulfur-deficient ore brines and the formation of exhalative base metal deposits. *Chem. Geol.* **2008**, *247*, 195–207. [CrossRef]
210. Relvas, J.M.R.S.; Barriga, F.J.A.S.; Longstaffe, F.J. Hydrothermal alteration and mineralization in the Neves-Corvo volcanic-hosted massive sulfide deposit, Portugal: II. Oxygen, hydrogen, and carbon isotopes. *Econ. Geol.* **2006**, *101*, 791–804. [CrossRef]
211. Mitsuno, C.; Nakamura, T.; Yamamoto, M.; Kase, K.; Oho, M.; Suzuki, S.; Thadeu, D.; Carvalho, D.; Arribas, A. *Geological Studies of the "Iberian Pyrite Belt" with Special Reference to Its Genetical Correlation of the Yanahara Ore Deposit and Others in the Inner Zone of Southwest Japan*; University of Okayama: Okayama, Japan, 1986; p. 300.
212. Kase, K.; Yamamoto, M.; Nakamura, T.; Mitsuno, C. Ore mineralogy and sulfur isotope study of the massive sulphide deposit of Filón Norte, Tharsis Mine, Spain. *Miner. Depos.* **1990**, *25*, 289–296. [CrossRef]
213. Velasco-Acebes, J.; Tornos, F.; Kidane, A.; Wiedenbeck, M.; Velasco, F. Strontium and sulfur isotopes reveal the complex evolution of the Sotiel-Migollas VMS deposit (Iberian Pyrite Belt). In Proceedings of the Goldschmidt Conference 2015, Prague, Czech Republic, 16–21 August 2015; p. 3252.
214. Eastoe, C.J.; Solomon, M.; García Palomero, F. A sulfur isotope study of the massive and stockwork pyrite deposits at Rio Tinto, Spain. *Trans. Inst. Min. Metall.* **1986**, *95*, 201–207.
215. Marcoux, E. Lead isotope systematics of the giant massive sulphide deposits in the Iberian Pyrite Belt. *Miner. Depos.* **1998**, *33*, 45–58. [CrossRef]
216. Pomiès, C.; Cocherie, A.; Guerrot, C.; Marcoux, E.; Lancelot, J. Pb/Pb isotopic ratio intercalibration with accurate U/Pb measurement. *Chem. Geol.* **1997**, *144*, 137–149. [CrossRef]
217. Nieto, J.M.; Almodóvar, G.R.; Pascual, E.; Sáez, R.; Jagoutz, E. Estudio isotópico con el sistema Re-Os de las mineralizaciones de sulfuros de la Faja Pirítica Ibérica. *Geogaceta* **1999**, *27*, 181–184.
218. Mathur, R.; Munk, L.A.; Townley, B.; Gou, K.Y.; Gómez Miguélez, N.; Titley, S.; Chen, G.G.; Song, S.; Reich, M.; Tornos, F.; et al. Tracing Low-Temperature Aqueous Metal Migration in Mineralized Watersheds with Cu Isotope Fractionation. *Appl. Geochem.* **2014**, *51*, 109–115. [CrossRef]

219. Viers, J.; Grande, J.A.; Zouiten, C.; Freydier, R.; Masbou, J.; Valente, T.; De la Torre, M.L.; Destrigneville, C.; Pokrovsky, O.S. Are Cu Isotopes a Useful Tool to Trace Metal Sources and Processes in Acid Mine Drainage (AMD) Context? *Chemosphere* **2018**, *193*, 1071–1079. [CrossRef] [PubMed]
220. Gaspar, M.; Relvas, J.M.R.S.; Carvalho, J.; Larsos, P.B.; Hart, G.; Pinto, A.; Pacheco, N.; Nipiva, P.C.; Barriga, G.; Santos, P. Cu Isotopic Variation in the Neves-Corvo Deposit, Iberian Pyrite Belt. *Geochim. Cosmochim. Acta* **2008**, *72*, 12.
221. Sáez, R.; Cardellach, E.; Moreno, C.; Almodovar, G.R.; Wasylenski, L.E.; Hui, A.K. Tracing Paleoenvironmental Conditions during Massive Sulphide Deposition in the Iberian Pyrite Belt (IPB): A Geochemical and Mo Isotope Approach. In Proceedings of the Goldschmidt Conference 2015, Prague, Czech Republic, 16–21 August 2015; Abstract. p. 2727.
222. Carvalho, D.; Barriga, F.J.A.S.; Munhá, J. Bimodal siliciclastic systems—The case of the Iberian Pyrite Belt. In *Volcanic-Associated Massive Sulphide Deposits: Processes and Examples in Modern and Ancient Settings*; Barrie, C.T., Hanningtonm, N.D., Eds.; Reviews in Economic Geology; SEG: Littleton, CO, USA, 1999; Volume 8, pp. 375–408.
223. Goodfellow, W.D.; Lydon, J.W.; Turner, R.W. Geology and genesis of stratiform sediment-hosted (SEDEX) Zn-Pb-Ag sulphide deposits. In *Mineral Deposit Modeling*; Kirkham, R.V., Sinclair, W.D., Thorpe, R.I., Duke, J.M., Eds.; Special Paper 40; Geological Association of Canada: St. John's, NF, Canada, 1993; pp. 201–251.
224. Hannington, M.D. Volcanogenic Massive Sulfide Deposits. In *Geochemistry of Mineral Deposits*, 2nd ed.; Scott, S.D., Ed.; Treatise on Geochemistry; Elsevier-Pergamon: Oxford, UK, 2014; pp. 463–488.
225. Tornos, F.; Peter, J.M.; Allen, R.; Conde, C. Controls on the Siting and Style of Volcanogenic Massive Sulphide Deposits. *Ore Geol. Rev.* **2015**, *68*, 142–163. [CrossRef]
226. Eickmann, B.; Baumberger, T.; Thorseth, I.H.; Strauss, H.; Früh-Green, G.L.; Pedersen, R.B.; Jaeschke, A. Sub-seafloor Sulfur Cycling in a Low-Temperature Barite Field: A Multi-Proxy Study from the Arctic Loki's Castle Vent Field. *Chem. Geol.* **2020**, *539*, 119495. [CrossRef]